Pharmacological Research 210 (2024) 107515

Contents lists available at ScienceDirect

Pharmacological Research

journal homepage: www.elsevier.com/locate/yphrs

PPARβ/δ prevents inflammation and fibrosis during diabetic cardiomyopathy

Adel Rostami [a,b,c,d,1], Xavier Palomer [a,b,c,d,*,1], Javier Pizarro-Delgado [a,b,c,d], Emma Barroso [a,b,c,d], Brenda Valenzuela-Alcaraz [e,f], Fátima Crispi [e,f], J. Francisco Nistal [g,h], María A. Hurlé [i], Raquel García [i], Walter Wahli [j,k,l], Manuel Vázquez-Carrera [a,b,c,d,*]

[a] Department of Pharmacology, Toxicology and Therapeutic Chemistry, Faculty of Pharmacy and Food Sciences, University of Barcelona, Barcelona 08028, Spain
[b] Institute of Biomedicine of the University of Barcelona (IBUB), University of Barcelona, Barcelona 08028, Spain
[c] Spanish Biomedical Research Center in Diabetes and Associated Metabolic Diseases (CIBERDEM)-Instituto de Salud Carlos III, Madrid 28029, Spain
[d] Pediatric Research Institute-Hospital Sant Joan de Déu, Esplugues de Llobregat 08950, Spain
[e] aBCNatal - Barcelona Center for Maternal-Fetal and Neonatal Medicine (Hospital Clínic and Hospital Sant Joan de Deu), Institut d'Investigacions Biomèdiques August Pi i Sunyer, Universitat de Barcelona, Barcelona, Spain
[f] Spanish Biomedical Research Center in Rare Diseases (CIBERER), Barcelona, Spain
[g] Servicio de Cirugía Cardiovascular, Hospital Universitario Marqués de Valdecilla, Instituto de Investigación Marqués de Valdecilla (IDIVAL), Departamento de Ciencias Médicas y Quirúrgicas, Facultad de Medicina, Universidad de Cantabria, Santander, Spain
[h] Spanish Biomedical Research Center in Cardiovascular Diseases (CIBERCV), Instituto de Salud Carlos III, Santander, Spain
[i] Departamento de Fisiología y Farmacología, Facultad de Medicina, Universidad de Cantabria, Instituto de Investigación Marqués de Valdecilla (IDIVAL), Santander, Spain
[j] Center for Integrative Genomics, University of Lausanne, Lausanne CH-1015, Switzerland
[k] Lee Kong Chian School of Medicine, Nanyang Technological University, Singapore 308232, Singapore
[l] ToxAlim (Research Center in Food Toxicology), INRAE, UMR1331, Cedex, Toulouse F-31300, France

ARTICLE INFO

Keywords:
Activator protein-1 (AP-1)
Diabetic cardiomyopathy
Fibrosis
Inflammation
Mitogen-activated protein kinases (MAPK)
Nuclear factor κB (NF-κB)

ABSTRACT

Diabetic cardiomyopathy (DCM) is a specific type of myocardial disease that often develops in patients suffering from diabetes, which has become the foremost cause of death among them. It is an insidious multifactorial disease caused by complex and partially unknown mechanisms that include metabolic dysregulation, local inflammation, fibrosis, and cardiomyocyte apoptosis. Despite its severity and poor prognosis, it often goes undiagnosed, and there are currently no approved specific drugs to prevent or even treat it. Peroxisome proliferator-activated receptor (PPAR)β/δ is a key metabolic regulator that has been proposed as a potential

Abbreviations: ADGRE1, adhesion G protein-coupled receptor E1 F4/80; AMPK, AMP-activated protein kinase; ANGPTL4, angiopoietin like 4; Ao PV, aorta peak velocity; Ao VTI, aortic velocity time integral aortic valve area; AP-1, activator protein-1; *APRT*, adenine phosphoribosyl transferase; BAX, BCL2 associated X; BCL2, B-cell CLL/lymphoma 2; BCL-XL, BCL2 like 1 BCL2L1; β-MHC, β-myosin heavy chain or MYH7, myosin heavy chain 7; BNP or NPPB, natriuretic peptide B; BW, body weight; CCL2, chemokine C-C motif ligand 2 or MCP1, monocyte chemoattractant protein; CCN2, cellular communication network factor 2 or *CTGF*, connective tissue growth factor; CHOP, C/EBP homologous protein; COL1A1, collagen type I alpha 1 chain; COL3A1, collagen type III alpha 1 chain; CT, control; CTGF, connective tissue growth factor or CCN2, cellular communication network factor 2; DCM, diabetic cardiomyopathy; DDIT3, DNA damage inducible transcript 3; DM1, type 1 diabetes; DM2, type 2 diabetes; EDN1, endothelin 1; EF, ejection fraction; ER, endoplasmic reticulum; ERK, extracellular signal-regulated kinase; FBS, fetal bovine serum; FS, fractional shortening; HG, hyperglycemia; HW, heart weight; IκBα, NF-κB inhibitor α; IL, interleukin; IVSd, interventricular septal wall thickness at end-diastole; IVSs, interventricular septal wall thickness at end-systole; JNK, c-Jun N-terminal kinase; KO, knockout; LGALS3, galectin 3; LV EDD, left ventricular end-diastolic diameter; LV ESD, left ventricular end-systolic diameter; MAPK, mitogen-activated protein kinase; MMP, matrix metallopeptidase or metalloproteinase; NF-κB, nuclear factor-κB; NPR1, natriuretic peptide receptor 1; NR1D1, nuclear receptor subfamily 1 group D member 1 or Rev-Erbα; PARP1, poly ADP ribose polymerase 1; PDK4, pyruvate dehydrogenase kinase 4; PPAR, peroxisome proliferator-activated receptor; PPRE, peroxisome proliferator response element; PWTd, left ventricular posterior wall thickness at end-diastole; PWTs, left ventricular posterior wall thickness at end-systole; ROS, reactive oxygen species; STAT3, signal transducer and activator of transcription 3; STZ, streptozotocin; TGFB1, transforming growth factor β1; TL, tibial length; TNF-α, tumor necrosis factor-α; TRIB3, tribbles pseudokinase 3; TRIM72, tripartite motif containing 72; WT, wild-type.

* Correspondence to: Department of Pharmacology, Toxicology and Therapeutic Chemistry, Faculty of Pharmacy, University of Barcelona, Av. Joan XXIII 27-31, Barcelona E-08028, Spain.
E-mail addresses: xpalomer@ub.edu (X. Palomer), mvazquezcarrera@ub.edu (M. Vázquez-Carrera).
[1] Both authors contributed equally.

https://doi.org/10.1016/j.phrs.2024.107515
Received 10 September 2024; Received in revised form 18 November 2024; Accepted 19 November 2024
Available online 20 November 2024

Peroxisome proliferator-activated receptor (PPAR)β/δ

target for DCM due to its pleiotropic anti-inflammatory properties. Diabetes was induced by multiple low-dose streptozotocin (STZ) administration in wild-type and PPARβ/δ knockout male mice treated with the PPARβ/δ agonist GW0742 or vehicle. Human cardiomyocytes (AC16) and mouse atrial myocytes (HL-1) exposed to hyperglycemia and treated with PPARβ/δ agonists were also used. PPARβ/δ deletion in mice negatively impacted cardiac morphology and function, which was accompanied by interstitial fibrosis and structural remodeling of the heart. This phenotype was further exacerbated in knockout diabetic mice. At the molecular level, PPARβ/δ suppression resulted in increased expression of pro-inflammatory and pro-fibrotic markers. Some of these markers were also induced by diabetes in wild-type mice and were exacerbated in diabetic knockout mice. The activity of the transcription factors nuclear factor κB (NF-κB) and activator protein-1 (AP-1) correlated with most of these changes. Remarkably, PPARβ/δ activation partially prevented inflammation and fibrosis in the heart, as well as cardiac atrophy, induced during diabetes in mice, and also in cultured cardiomyocytes exposed to hyperglycemia. Finally, our results suggest that the beneficial effects of PPARβ/δ activation are mediated by the inhibition of mitogen-activated protein kinases (MAPK) activity and subsequent downregulation of the transcriptional activities of NF-κB and AP-1. Overall, the data suggest that PPARβ/δ agonists might be useful in preventing inflammation and fibrosis progression in DCM.

1. Introduction

Patients suffering from diabetes may develop a type of myocardial remodeling that is not directly attributable to hypertension, coronary artery disease, or valvular heart disease, and which is referred to as diabetic cardiomyopathy (DCM). The prevalence of this condition ranges from 20 % to 60 % among the diabetic population and affects both patients with type 1 (DM1) and type 2 (DM2) diabetes mellitus [1–3]. The pathophysiological mechanisms underlying DCM are multifactorial and partially unknown, although it is widely accepted that hyperglycemia plays a pivotal role [4]. During diabetes, attenuation of insulin signaling promotes mitochondrial fatty acid β-oxidation as the sole fuel source instead of glucose [5]. Despite the higher fatty acid oxidation rate, myocardial lipid accumulation and ensuing accumulation of toxic lipid intermediates (lipotoxicity) occur. Cardiac steatosis is currently regarded as a significant cause of DCM [6,7]. Both hyperglycemia and lipotoxicity activate nuclear factor κB (NF-κB) in cardiomyocytes, and the resultant increased expression and secretion of pro-inflammatory mediators exerts several autocrine deleterious effects via downstream activation of activator protein-1 (AP-1) and NF-κB itself [6,8]. Myocardial injury caused by these inflammatory processes is actively involved in the development of cardiac remodeling. Interstitial fibrosis, which occurs due to excess deposition of extracellular matrix [9], is a hallmark of myocardial remodeling during DCM, and is considered a primary determinant of dysfunctional cardiac performance. NF-κB and AP-1 are part of the complex network of transcription factors involved in regulating extracellular matrix protein homeostasis.

Hyperglycemia and undue fatty acid oxidation during DCM promote excess reactive oxygen species (ROS) generation by cardiomyocytes, which leads to the uncoupling of oxidative metabolism, induces oxidative damage in DNA, proteins and lipids, triggers NF-κB activation and gives rise to endoplasmic reticulum (ER) stress and mitochondrial dysfunction [3,4,10]. Consequently, myocardial energy generation is impaired, calcium handling is disturbed, cardiac contractility and efficiency are reduced, and cardiomyocyte apoptosis is hastened [3,10–12]. There is also apoptosis that originates from several mechanisms, including the activation of DNA reparative enzymes such as poly ADP ribose polymerase 1 (PARP1) [10]. PARP1 activates NF-κB and suppresses the glycolytic pathway, thus favoring hyperglycemia-induced cell injury. Overall, these changes result in extracellular cardiac remodeling, contractile dysfunction, left ventricular hypertrophy, and dilated cardiomyopathy, thus reducing cardiac output and eventually leading to heart failure, the foremost cause of death in diabetic patients [6].

Interestingly, a growing body of evidence points to a potential link between chronic low-grade inflammation, fibrosis and metabolic dysregulation during cardiac diseases [6]. At the transcriptional level, cardiac metabolism is mainly regulated by the peroxisome proliferator-activated receptor (PPAR) nuclear receptor subfamily, which via its transcriptional targets plays a central role in DCM [13]. The PPAR subfamily consists of three receptor subtypes: PPARα, PPARβ/δ and PPARγ. PPARβ/δ, which is the principal form in cardiac cells, is a key metabolic regulator with pleiotropic anti-inflammatory properties and potential anti-diabetic effects. PPARβ/δ activation may attenuate pro-inflammatory signaling pathways through different mechanisms and, as such, interferes with cardiac remodeling [6,14–16]. However, little is known about the role of PPARβ/δ in DCM, or the potential effects of PPARβ/δ agonists to treat this disease. The main goal of the present study was to investigate the potential protective role of PPARβ/δ in the heart by examining the effects of this nuclear receptor in streptozotocin (STZ)-induced type 1 diabetic mice and in cultured cardiac cells under hyperglycemia conditions.

2. Materials and methods

2.1. Reagents

GW0742 (#10006798) was from Cayman Chemical Company (Ann Arbor, MI, USA). All other chemicals, except when indicated, were purchased from Sigma-Aldrich Corporation (St. Louis, MO, USA): glucose (G7021), GW501516 (SML1491), mannitol (M9546), SB202190 (S7067), SP600125 (S5567), Streptozotocin (S0130), and U0126 (#662005).

2.2. Mouse cardiac sample preparation

Twelve-week-old male PPARβ/δ knockout (KO) mice and their control wild-type (WT) littermates with the same genetic background (C57BL/6×129/SV) were used. Each strain was randomized into two groups: animals in the diabetic groups were injected with STZ (50 mg/kg) intraperitoneally for five consecutive days, whereas animals in the control group received vehicle (0.1 M sodium citrate buffer, pH 4.5). The multiple low-dose STZ-induced diabetes is a well-established model that develops type 1 diabetes and eventually DCM [17], and does not produce non-specific toxicity in animals [18]. After two weeks, mice with a blood glucose value of ≥250 mg/dL were considered diabetic. Mice were housed under standard light-dark cycle (12-h light/dark cycle) and temperature (21 ± 1ºC) conditions, and food and water were provided *ad libitum*. The hearts were collected 24 weeks after the diagnosis of diabetes from mice euthanized using deep isoflurane (5 %) anesthesia, rinsed in ice-cold phosphate buffer saline, and snap-frozen in liquid nitrogen.

To establish the role of PPARβ/δ activation, diabetes was induced in C57BL/6 mice by intraperitoneal administration of STZ as described above, and then mice were fed a regular chow diet (Harlan Ibérica S.A.) for the next 16 weeks supplemented, or not, with the PPARβ/δ agonist GW0742 (0.0012 % w/w, equivalent to an approximate daily dose of 1 mg/kg per day). This time treatment was used to specifically examine

the potential prophylactic effects of PPARβ/δ activation on the development of DCM. At this dose, GW0742 activates PPARβ/δ, but not PPARα or PPARγ [19]. Samples were collected as described before.

All animal procedures were approved by the Institutional Animal Care and Use Committee of the University of Barcelona (231/22-P1), as stated in Law 5/21 July 1995, passed by the Generalitat de Catalunya. All experiments were performed in accordance with EU recommendations (Directive 2010/63/EU) for experimental design and analysis in pharmacology care, and followed the ARRIVE and standard ethical guidelines [20]. Accordingly, all efforts were made to minimize the suffering and the number of mice used.

2.3. Transthoracic echocardiography of mice

Mice were sedated using a mixture of isoflurane (5 %) and oxygen (2 L/min), which was subsequently reduced to 1.5 % isoflurane to maintain the heart rate in the range of 350–450 beats/min. Transthoracic echocardiography was performed from a longitudinal parasternal plane using a Vivid Q (GE Healthcare, Norway) echocardiograph equipped with a 5.0–13.0 MHz 33 mm linear probe. The acquired images' offline analysis was used to determine ejection fraction (EF), shortening fraction (SF), septal and left ventricular free wall thicknesses, and end diastolic and end systolic diameters by M-mode.

2.4. Blood pressure and heart rate

According to the manufacturer's instructions, blood pressure and heart rate were measured in conscious mice using the tail-cuff method (BP2000; Visitech Systems, Drammen, Norway). Briefly, mice were first trained for five days, and then ten consecutive measurements were averaged to calculate systolic, diastolic and mean arterial blood pressure and heart rate.

2.5. Histology

Hearts were fixed in 4 % buffered paraformaldehyde and paraffin-embedded for subsequent hematoxylin and eosin or Masson's trichrome stains. Myocardial transverse sections (5 μm thick) were visualized using an Olympus BX41 microscope equipped with a DP11 CCD camera (Olympus Iberia, Barcelona, Spain), and digital images were obtained at 200x magnification. The cardiomyocyte cross-sectional area was analyzed in approximately 50 cells of two randomly chosen sections per mouse using ImageJ software (National Institutes of Health, USA). The degree of fibrosis was determined in two randomly chosen frames from Masson's trichrome-stained sections, and the area of fibrosis was determined using ImageJ software. The percentage of interstitial fibrotic areas was calculated as the fraction of the light-blue–stained area×100 %.

2.6. Cell culture

The human AC16 cell line, which develops many biochemical and morphological properties characteristic of cardiac muscle cells, was grown as previously described [21]. Briefly, non-differentiated AC16 cardiomyocytes (Merck Millipore, Burlington, MA, USA) were maintained in a medium composed of Dulbecco's modified Eagle's medium (DMEM) (Life Technologies, Spain) supplemented with 10 % fetal bovine serum (FBS), 1 % penicillin-streptomycin and 1 % Fungizone (Life Technologies). The mouse atrial myocyte cell line (HL-1, Merck Millipore) was cultured at 37°C in DMEM with 10 % FBS and 1 % penicillin-streptomycin. Human cardiac fibroblasts (HCF) isolated from adult healthy hearts were provided by Innoprot (#P10452; Derio, Spain), and cultured following the manufacturer's procedures. HCF cells were grown in Fibroblast Medium-2 supplemented with 5 % FBS and 1 % penicillin-streptomycin. All cell lines were grown at 37ºC in a humid atmosphere of 5 % CO2/95 % air, and the experiments were conducted at approximately 80 % cell confluency. To establish the cellular model of diabetes, cells were maintained in hyperglycemia (HG) medium with 30 (HL-1) or 50 (AC16 and HCF) mM glucose and 0.5 % (HCF) or 2 % (AC16 and HL-1 cells) FBS for different time treatments. Cells cultured under normal medium containing 1 mM glucose were set as the control group (CT). Additional mannitol was included in the CT group medium as an osmotic control. To elucidate the role of PPARβ/δ, cells were pre-incubated with the PPARβ/δ agonists GW501516 (10 μM, AC16 and HCF) or GW0742 (1 μM, HL-1) for 24 h, and freshly added each 24 additional h. Experiments were repeated at least two times.

2.7. Human samples

This study was carried out using left ventricular myocardial intraoperative biopsies obtained from a cohort of 19 diabetic patients (5 women) who were diagnosed with isolated severe aortic stenosis and underwent aortic valve replacement surgery in the University Hospital Marqués de Valdecilla in Santander (Spain). Patients with aortic or mitral regurgitation greater than mild or with major coronary stenosis >50 %, previous cardiac operations, malignancies, or poor renal or hepatic function were deemed ineligible for the study. Subepicardial biopsies were taken from the left ventricular lateral wall with a Tru-cut needle during the surgical procedure. Samples were all harvested by the same surgeon in a protocolized manner and always from the same location in the margo obtusus of the heart. The study followed the Declaration of Helsinki guidelines for biomedical research involving human subjects. The Institutional Ethics and Clinical Research Committee of Cantabria approved the study (PI21/00084), and all patients provided written informed consent.

2.8. RNA preparation and analysis

Total RNA was isolated using Ultraspec reagent (Biotecx, Houston, TX, USA). RNA samples were cleaned (NucleoSpin RNA; Macherey-Nagel, Düren, Germany) and checked for integrity by agarose gel electrophoresis. The total RNA isolated by this method was undegraded and free of protein and DNA contamination. Relative levels of specific mRNAs were assessed by real-time RT-PCR as previously described [22]. Reverse transcription was performed from 0.5 μg total RNA using Oligo $(dT)_{23}$ and M-MLV Reverse Transcriptase (Life Technologies). The PCR reaction contained 10 ng of reverse-transcribed RNA, 2X IQ™ SYBR-Green Supermix (Bio-Rad, Barcelona, Spain) and 900 nM of each primer. PCR assays were performed on a BioRad MiniOpticon™ Real-Time PCR system. Thermal cycling conditions were as follows: activation of Taq DNA polymerase at 95ºC for 10 minutes, followed by 40 cycles of amplification at 95ºC for 15 seconds and at 60ºC for 1 minute. Optimal amplification efficiency for each primer set was assessed, and a dissociation protocol was carried out to ensure a single PCR product. The sequences of the forward and reverse primers used for amplification are shown in supplementary Table S1.

2.9. Immunoblot analysis and coimmunoprecipitation studies

To obtain total protein extracts, AC16 cardiac cells or frozen tissue slides were lysed in cold RIPA buffer containing phosphatase and protease inhibitors (5.4 μg/mL aprotinin, 20 μg/mL leupeptin, 0.2 mM phenylmethylsulfonyl fluoride, 1 mM sodium orthovanadate, 5 mM sodium floride). The homogenate was then centrifuged at 10,000×*g* for 30 min at 4°C, and the supernatant protein concentration was determined using the Pierce BCA protein assay kit (Thermo Fisher Scientific, Waltham, MA, USA). Isolation nuclear fractions was performed as follows: AC16 cardiac cells or homogenized cardiac slides were incubated on ice for 30 min in buffer A (10 mM HEPES, pH 7.9, 10 mN KCl, 0.2 mM EDTA, 1 mM dithiothreitol, plus phosphatase and protease inhibitors) containing 0.625 % Nonidet P-40. Cell lysates were centrifuged at 4°C, 10,000×*g* for 1 min, and supernatants were stored as cytosolic fraction.

Pellets were suspended in buffer B (20 mM HEPES, pH 7.9, 0.42 M NaCl, 2 mM EDTA and 1 mM dithiothreitol, with phosphatase and protease inhibitors), centrifuged at 4°C, 13,000×*g* for 5 min, and the resultant supernatant (nuclear extract) stored at −80°C. Protein concentration was determined using the Pierce BCA protein assay kit. For immunoblotting, protein fractions were separated by sodium dodecyl sulfate-polyacrylamide gel electrophoresis (SDS-PAGE) on 10 % separation gels and transferred to Immobilon polyvinylidene difluoride membranes. Proteins were detected with several antibodies (see supplementary Table S2) using the Western Lightning® Plus-ECL chemiluminescence kit (Thermo Fisher Scientific) and their size was estimated using protein molecular mass standards (Life Technologies).

For coimmunoprecipitation studies, total protein extracts (25 μg) and 4 μg of the primary antibody were brought to a final volume of 300 μL with dilution buffer (25 mM Tris-HCl pH 7.4, 150 mM NaCl, 1 mM EDTA, 1 % NP-40, 5 % glycerol, 2 % BSA) and incubated for 18 h at 4ºC under gentle agitation. Immunocomplexes were captured by adding 50 μL of Protein A/G Plus Agarose beads (Santa Cruz Biotechnology, Inc.) to the samples and incubating 6 h at 4ºC under rotary agitation. Agarose beads were collected by centrifugation and washed three times with PBS. Finally, the protein was eluted with SDS-PAGE sample buffer, and the resultant supernatant was subjected to electrophoresis and immunoblotted with the corresponding antibodies.

2.10. NF-κB p65 and AP-1 DNA-binding activity assay

The DNA-binding activities of p65/NF-κB and FOS/AP-1 in nuclear extracts were examined using the p65/NF-κB and FOS/AP-1 transcription-factor-assay kits (ab133112 and ab207196, respectively; Abcam, Cambridge, UK). The assays were performed accordingly to the manufacturer's protocols. The DNA binding activity was calculated as a fold of control.

2.11. Statistical analysis

Statistical differences were established by either the Student's t-test or two-way ANOVA, according to the number of groups compared. The parametric Pearson coefficient correlation was used to calculate the correlation for continuous variables using only complete pairs of observations. Before analysis, the normality and homoscedasticity of data distribution were checked by Shapiro-Wilk and Bartlett tests, respectively. Statistical analyses were performed with GraphPad Prism 10 software (GraphPad Software Inc., San Diego, CA, USA). Values of $P < 0.05$ were considered statistically significant.

3. Results

3.1. PPARβ/δ deletion negatively impacts cardiac morphology during DCM in mice

At sacrifice, glycemia was comparable between WT and KO diabetic mice, and was significantly higher than that of non-diabetic mice (Table 1). This hyperglycemia was maintained throughout the study period in both groups of diabetic mice (see supplementary Fig. S1A). In conscious diabetic WT and KO mice, heart rate was reduced compared to non-diabetic littermates (Table 1). In contrast, blood pressure was not significantly modified by diabetes but by PPARβ/δ deletion. Even though hypertension is a common feature of diabetes, some studies have revealed that STZ-induced diabetes has no significant effect on blood pressure in most of the mice strains examined, including C57BL/6. In contrast, other authors reported lower systolic blood pressure after STZ administration [23]. However, in agreement with our results, a reduced heart rate was reported by others [18,24].

We did not find significant differences in the ejection fraction (EF) or fractional shortening (FS) in these mice (Table 1). A significant increase in left ventricular end-diastolic diameter (LV-EDD) was evident in WT diabetic and PPARβ/δ KO mice (both diabetic and non-diabetic) compared to non-diabetic WT mice (Table 1). Left ventricular end-systolic diameter (LV-ESD) also augmented slightly, but it did not reach statistical significance. Left ventricular posterior wall thickness at end diastole (PWTd) and systole (PWTs) and interventricular septal wall thickness at end-diastole (IVSd) and systole (IVSs) were increased in normoglycemic KO mice but not in diabetic WT mice, nor after inducing diabetes in PPARβ/δ KO mice (Table 1). The augmented aortic velocity time integral (Ao VTI) and aorta peak velocity (Ao PV) in KO mice compared to WT mice, and particularly in KO diabetic mice, together with the absence of changes in EF and heart rate (Table 1), suggest the occurrence of increased cardiac output in KO mice.

Table 1
Biochemical, biometric, echocardiographic and hemodynamic variables of wild-type (WT) or PPARβ/δ knockout (KO) male mice at 6 months after the onset of diabetes. Diabetes was induced by intraperitoneal injection of streptozotocin (STZ; 50 mg/kg body weight) for five consecutive days. Mice serving as controls were given the same volume of sodium citrate 0.1 M pH 4.5.

	Group			
Parameter	WT	WT+STZ	PPARβ/δ KO	KO+STZ
Glycemia (mg/dL)	138.0 ± 18.3	477,8 ± 129.2$^{***,\#\#\#}$	142.6 ± 21.6	479.2 ± 120.5$^{***,\#\#\#}$
Body weight (g)	37.1 ± 4.7	30.6 ± 3.5*	34.4 ± 5.2	24.8 ± 4.2$^{***,\#\#\#}$
Heart weight (mg)	141.7 ± 6.1	129.3 ± 16.2	129.3 ± 19.5	95.5± 7.4$^{***,\&\&\&,\#\#\#}$
HW/BW (mg/g)	3.96 ± 0.49	4.35 ± 0.29	3.74 ± 0.44	3.95 ± 0.70
HW/TL (mg/mm)	7.87 ± 0.54	7.00 ± 1.03	7.53 ± 1.30	5.37 ± 0.36$^{***,\&,\#\#\#}$
EF (%)	67.9 ± 7.2	61.9 ± 13.8	67.3 ± 13.3	66.5 ± 6.0
FS (%)	32.6 ± 5.4	29.3 ± 8.8	33.4 ± 9.5	31.7 ± 4.6
IVSd (mm)	0.74 ± 0.10	0.70 ± 0.08	0.91 ± 0.11*	0.68 ± 0.17$^{\#\#}$
IVSs (mm)	0.87 ± 0.10	0.91 ± 0.13	1.14 ± 0.12*	0.90 ± 0.18$^{\#}$
PWTd (mm)	0.70 ± 0.14	0.70 ± 0.15	0.94 ± 0.15*	0.70 ± 0.11$^{\#}$
PWTs (mm)	0.91 ± 0.17	0.88 ± 0.12	1.24 ± 0.22**	0.84 ± 0.15$^{\#\#}$
LV EDD (mm)	2.84 ± 0.51	3.64 ± 0.62*	3.55 ± 0.48*	3.63 ± 0.36*
LV ESD (mm)	1.96 ± 0.31	2.55 ± 0.75	2.41 ± 0.31	2.38 ± 0.37
Ao VTI (mm2)	3.21 ± 1.02	3.59 ± 1.55	4.97 ± 1.35*	5.92 ± 1.28$^{**,\&}$
Ao PV (mm/sec)	0.77 ± 0.17	0.87 ± 0.17	1.04 ± 0.20*	1.12 ± 0.11**
Systolic BP (mmHg)	109.1 ± 7.1	99.8 ± 14.2	92.4 ± 18.4*	96.2 ± 14.2
Diastolic BP (mmHg)	50.5 ± 10.6	54.6 ± 13.1	48.4 ± 11.3	43.1 ± 6.4*
Mean BP (mmHg)	69.8 ± 7.0	69.9 ± 12.0	62.9 ± 13.1*	62.0 ± 7.5*
Heart rate (bpm)	687 ± 45	603 ± 35*	675 ± 37	577 ± 50$^{**,\#\#}$

Data indicate median ± SD (n = 8–10 mice per group).
Abbreviations: BP, blood pressure; BW, body weight; HW, heart weight; TL, tibial length; EF, ejection fraction; FS, fractional shortening; IVSd, interventricular septal wall thickness at end-diastole; IVSs, interventricular septal wall thickness at end-systole; PWTd, left ventricular posterior wall thickness at end-diastole; PWTs, left ventricular posterior wall thickness at end-systole; LV EDD, left ventricular end-diastolic diameter; LV ESD, left ventricular end-systolic diameter; Ao VTI, aortic velocity time integral (aortic valve area); Ao PV, aorta peak velocity.
$^{*}P<0.05$, $^{**}P<0.01$ and $^{***}P<0.001$ vs. WT; $^{\&}P<0.05$, $^{\&\&}P<0.01$ and $^{\&\&\&}P<0.001$ vs. WT+STZ; $^{\#}P<0.05$, $^{\#\#}P<0.01$ and $^{\#\#\#}P<0.001$ vs. PPARβ/δ KO.

Next, we sought to determine whether functional alterations observed in diabetic and PPARβ/δ KO corresponded to cardiac structural remodeling. As previously reported [25], the multidose STZ protocol caused a significant reduction of absolute heart weight (HW), although it only reached statistical significance in KO mice (Table 1). Likewise, administration of STZ, particularly in mice lacking PPARβ/δ, resulted in decreased body weight (BW) gain compared with age-matched controls, a fact which is a hallmark of this model of type 1 diabetes [23,26]. This might account for the lack of significant HW/BW relationship changes in diabetic mice. In contrast, the ratio HW/tibial length (TL) was diminished in diabetic mice, particularly in those lacking the *Pparβ/δ* gene, thus confirming the lack of cardiac hypertrophy in these mice. TL is a suitable surrogate that intends to avoid biases because of disease-induced BW changes, but a recent study has cast doubt about the mathematical suitability of the HW/TL relationship in small animal models, and has proposed the ratio HW/TL^3 as a more reliable marker [27]. Nevertheless, in our study the relationship HW/TL^3 also diminished in diabetic KO mice (supplementary Fig. S1B). As described above, diabetic mice displayed dilation of the cavity diameter (LV EDD) without an increase in parietal thickness, a geometric pattern that suggests the existence of eccentric hypertrophy. Thus, we next estimated the LV mass according to the method of Deveraux *et al.* [28]. As it is shown in supplementary Fig. S1C and D, the estimated LV mass was not significantly increased in diabetic mice, nor was the estimated LV mass/BW ratio. Lastly, H&E staining showed that the myocardial fibers were arranged regularly, and no differences were found in cardiomyocyte size between groups (Fig. 1A/B). Masson's trichrome staining showed fibrosis in KO and diabetic mice compared to non-diabetic WT mice (Fig. 1C/D). In particular, the KO diabetic group showed robust cardiac fibrosis, as well as destroyed and disorganized collagen network structure in the interstitial and perivascular areas.

3.2. *PPARβ/δ deletion favors inflammation, fibrosis and apoptosis during DCM in mice*

To gain further insight into the mechanisms underlying the aforementioned changes, we examined several components of the inflammation and fibrosis signaling pathways in the heart of these mice. PPARβ/δ deletion in mice resulted in spontaneous increased expression of some cardiac proinflammatory and profibrotic markers compared with their control littermates (Fig. 2A, and supplementary Fig. S2A-C). These included chemokine (C-C motif) ligand 2 (*Ccl2*, also referred to as monocyte chemoattractant protein 1 or *Mcp1*), collagen type I alpha 1 chain (*Col1a1*), galectin 3 (*Lgals3*), interleukin 1β (*Il1b*), *Il10*, matrix metallopeptidase 9 (*Mmp9*), nuclear receptor subfamily 1 group D member 1 (*Nr1d1* or Rev-Erbα), tripartite motif containing 72 (*Trim72*), or tumor necrosis factor (*Tnf*)-*α*. This pro-inflammatory profile was not a consequence of increased macrophage infiltration in the heart, as suggested by the absence of changes in the expression of adhesion G protein-coupled receptor E1 (*Adgre1*, or *F4/80*) and *Cd68* antigen, which

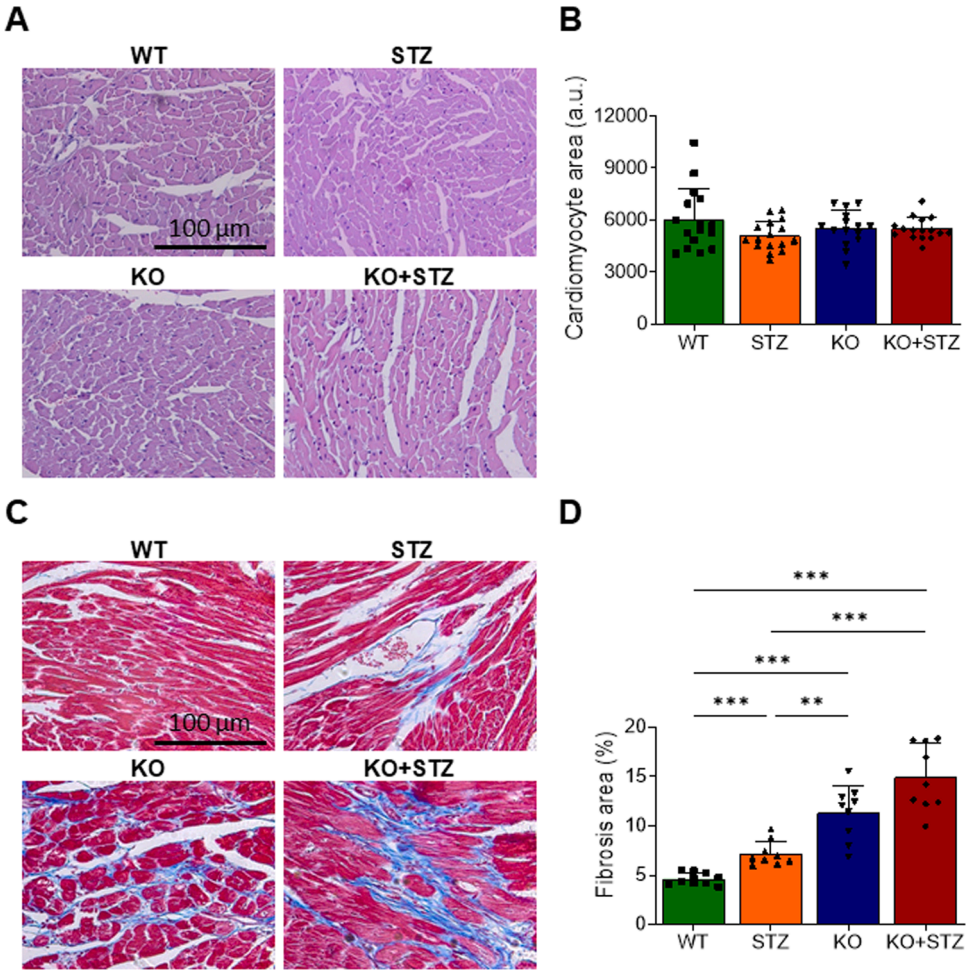

Fig. 1. PPARβ/δ suppression boosts cardiac fibrosis in STZ-induced diabetic mice. Representative hematoxylin and eosin-stained micrographs (A) showing transverse sections from the left ventricle myocardium and quantification of cardiomyocyte cross-sectional areas (B) in PPARβ/δ knockout (KO) mice and their wild-type (WT) littermates with (STZ) or without diabetes. Representative images of Mason's trichrome staining (C) and quantification of fibrosis expressed as a percentage of WT samples in the heart (D) of the same animal groups. Data are presented as the mean ± SD (n = 8–10 mice per group). $^{*}P < 0.05$, $^{**}P < 0.01$, $^{***}P < 0.001$.

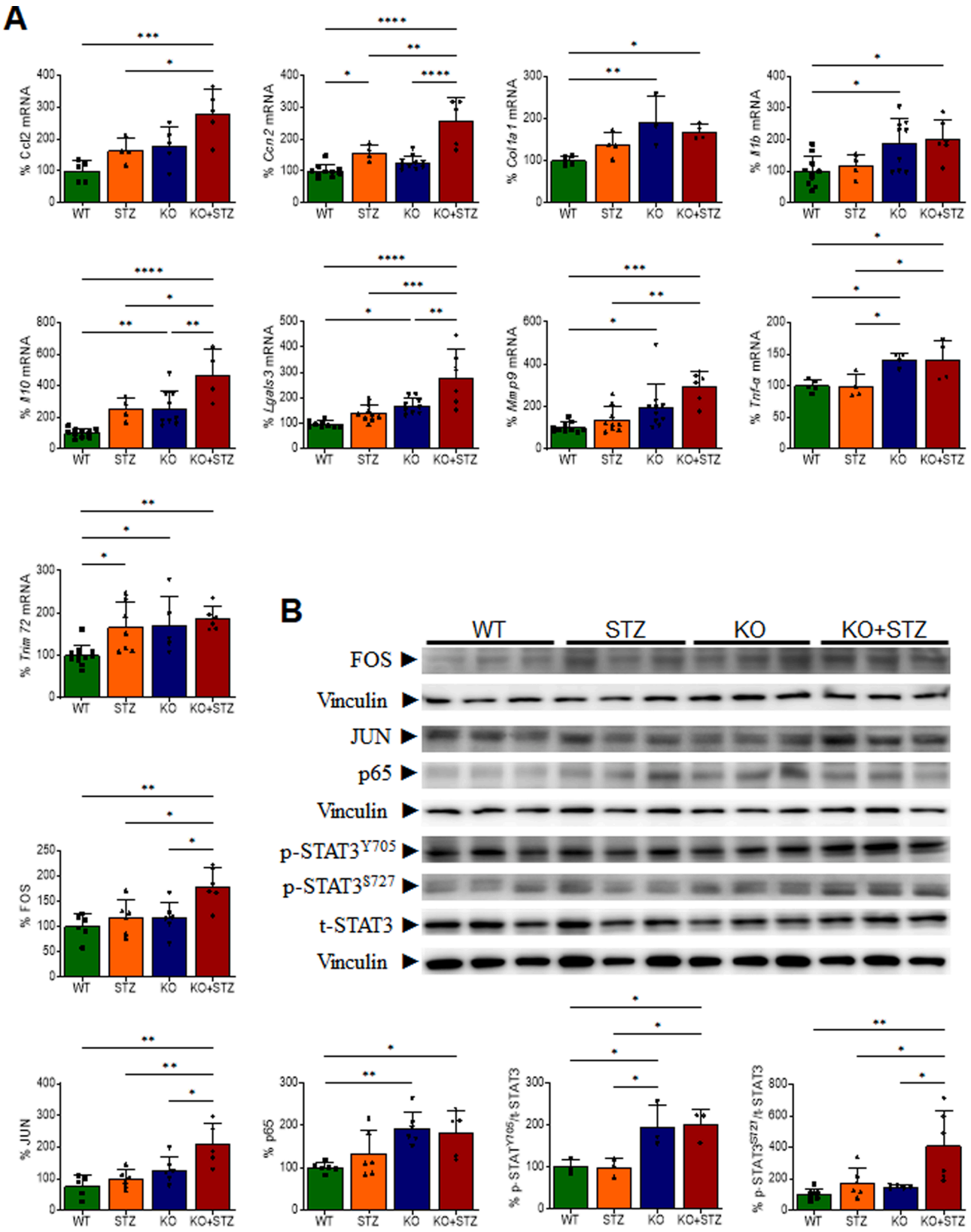

Fig. 2. PPARβ/δ deletion favors inflammation and fibrosis during DCM in mice. (A) Relative quantification of the mRNA expression of *Ccl2*, *Ccn2*, *Col1a1*, *Il1b*, *Il10*, *Lgals3*, *Mmp9*, *Tnf-α*, and *Trim72* and (B) Western blot analysis showing the protein levels of FOS, JUN, p65, p-STAT3^{Y705}/STAT3, and p-STAT3^{S727}/STAT3 in PPARβ/δ knockout (KO) mice and their wild-type (WT) littermates with (STZ) or without diabetes. The graphs represent the quantification of adenine phosphoribosyl transferase (*Aprt*)-normalized mRNA levels (A) or the normalized quantification of protein levels (B) expressed as a percentage of the control samples. Data are presented as the mean ± SD (n = 6–10 mice per group). $^{*}P < 0.05$, $^{**}P < 0.01$, $^{***}P < 0.001$.

are widely used as macrophage-specific markers (supplementary Fig. S2D). Some of the pro-inflammatory markers (*Ccl2*, *Il10*, and *Trim72*) were also induced by STZ-induced diabetes in WT mice, and even more in diabetic PPARβ/δ knockout mice (Fig. 2A). At the same time, cellular communication network factor 2 (*Ccn2* or *Ctgf*, connective tissue growth factor) was upregulated only after diabetes induction. The gene expression of *Col3a1* (collagen type III alpha 1 chain) was only induced in diabetic knockout mice, while *Mmp2* and *Tgfb1* (transforming growth factor β1) were not modified by any of these treatments (supplementary Fig. S2C). The hearts of PPARβ/δ KO mice displayed increased levels of the p65 subunit of NF-κB, although hyperglycemia had no effect (Fig. 2B). In contrast, the hearts of KO and diabetic mice displayed a trend to increase the levels of the FOS and JUN subunits of AP-1, although it only reached statistical significance in diabetic KO mice. The signal transducer and activator of the transcription 3 (STAT3) was also activated in KO mice, particularly in those that had diabetes, as demonstrated by the enhanced phosphorylation at Tyr705 and Ser727 residues (Fig. 2B).

We next assessed the expression of molecular markers of cardiac hypertrophy. As previously reported [29,30], we observed an increase in the expression of natriuretic peptide B (*Nppb* or *Bnp*) and myosin heavy chain 7 (*Myh7* or β-myosin heavy chain, *β-Mhc*) in diabetic mice compared with WT control animals (Fig. 3A). However, in the latter case it did not reach significance. Strikingly, *Nppb* expression was strongly reduced in KO mice regardless of whether they were diabetic. *Akt3* (AKT serine/threonine kinase 3), the sustained increase of which has been related to maladaptive hypertrophy [31], was also increased in PPARβ/δ knockout mice, but not after diabetes induction. The expression of natriuretic peptide receptor 1 (*Npr1*) did not change significantly in any of the groups (supplementary Fig. S2E). Since we did not find changes in cardiomyocyte size between groups (Fig. 1B), we explored whether the reduction in cardiomyocyte number could account for the decrease in

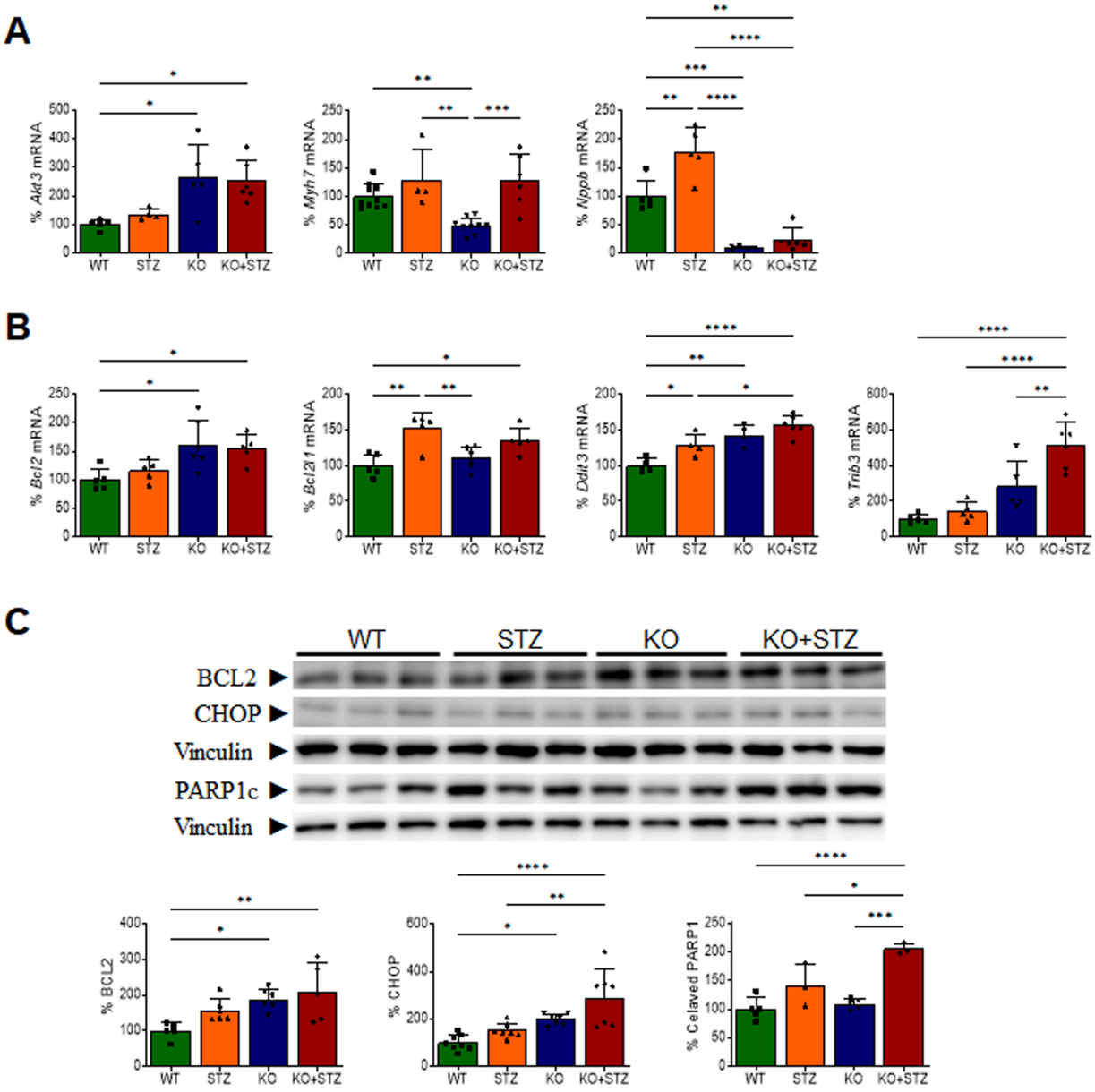

Fig. 3. Cardiac apoptotic markers are induced in diabetic and PPARβ/δ KO mice. Relative quantification of the mRNA expression of *Akt3*, *Myh7*, and *Nppb* (A) and *Bcl2*, *Bcl2l1*, *Ddit3*, and *Trib3* (B) in PPARβ/δ knockout (KO) mice and their wild-type (WT) littermates with (STZ) or without diabetes. C Western blot analysis shows the BCL2, CHOP, and PARP1c protein levels in the same animal groups. The graphs represent the quantification of adenine phosphoribosyl transferase (*Aprt*)-normalized mRNA levels (A and B) or the normalized quantification of protein levels (C) expressed as a percentage of the control samples. Data are presented as the mean ± SD (n = 6–10 mice per group). $^{*}P < 0.05$, $^{**}P < 0.01$, $^{***}P < 0.001$.

cardiac mass observed throughout our experiments, as demonstrated before [12]. Thus, we analyzed the mitochondria-dependent apoptotic cell death pathway, which is predominant in this diabetic model [32]. The gene expression of *Bax* (BCL2 associated X) was not modified, but *Bcl2* (B-cell CLL/lymphoma 2) and *Bcl2l1* (BCL2 like 1 or *Bcl-XL*) were induced in the heart of KO or diabetic mice, respectively (Fig. 3B). Likewise, the mRNA levels of both *Ddit3* (DNA damage inducible transcript 3) and *Trib3* (tribbles pseudokinase 3) where upregulated by STZ treatment or PPARβ/δ suppression (Fig. 3B). Western-blot analysis revealed that BCL2 and CHOP (C/EBP homologous protein, encoded by the *Ddit3*, gene) protein levels were also induced by diabetes and PPARβ/δ suppression in KO mice, while cleaved PARP1 increased only in STZ-treated mice (Fig. 3C).

3.3. The PPARβ/δ agonist GW0742 partially prevents inflammation and fibrosis induced during DCM in mice

To further confirm the role of PPARβ/δ during DCM, multiple low-dose STZ-induced diabetic mice and age-matched controls were treated with the PPARβ/δ agonist GW0742 or a vehicle. The gene expression of the PPARβ/δ transcriptional target *Angptl4* (angiopoietin like 4) was used to confirm the effect of GW0742 on this nuclear receptor throughout our experiments (supplementary Fig. S3A). *Angptl4* mRNA levels were also induced by STZ treatment in the heart of WT mice, where it might regulate processes associated with inflammation, oxidative stress, or lipid metabolism [33]. Treatment with GW0742 did not alter the hyperglycemic state, food consumption, or water intake of the STZ-treated animals, but it totally or partially prevented the decrease in heart weight, and the HW/BW and HW/TL ratios observed in diabetic mice (Table 2 and supplementary Fig. S3B). In agreement with previously published data [24], GW0742 partially prevented body weight reduction and, interestingly, its administration to non-diabetic mice did not yield any change in these parameters compared to the control animals.

No differences were found in cardiomyocyte size between groups (Fig. 4A and B). Furthermore, according to echocardiographic data and blood pressure measurements, no significant functional or morphological alterations were found in STZ-induced diabetic mice, nor after GW0742 treatment (Table 2). As described above, the heart rate was reduced in diabetic mice compared to non-diabetic littermates. Masson's trichrome staining demonstrated that GW0742 treatment prevented the increase in the fibrotic area observed in STZ-induced diabetic mice (Fig. 4C and D). Remarkably, the pro-inflammatory and pro-fibrotic response displayed after inducing diabetes in mice was partially abolished by GW0742 treatment, since this drug reduced the expression of *Il1b* and *Ccl2*, *Ccn2*, *Col1a1*, endothelin 1 (*Edn1*) and *Trim72* (Fig. 5A). However, no changes were observed in the mRNA levels of other pro-inflammatory and pro-fibrotic (*Il10*, *Tnf-α*, *Mmp9*) markers after GW0742 treatment (supplementary Fig. S3C), nor in the expression of genes related to cardiac hypertrophy (*Nppb*, *Myh7*; supplementary Fig. S3D), suggesting that this nuclear receptor is not directly involved in these effects. Following this, PPARβ/δ activation by GW0742 prevented the rise of p65 and the activation of STAT3 induced by STZ in the heart of mice (Fig. 5B). Similar to the results obtained with the PPARβ/δ KO mice, STZ treatment alone did not statistically increase FOS and JUN protein levels and, thus, GW0742 treatment had no effect either. Although GW0742 did not reduce gene expression of apoptotic markers (*Bcl2*, *Bcl2l1*, *Ddit3*, *Trib3*; supplementary Fig. S3E), it prevented the STZ-induced increase of cleaved PARP1 (Fig. 5B).

3.4. PPARβ/δ activation prevents the inflammatory and fibrotic profiles induced by hyperglycemia in vitro

First, we used the human AC16 cardiomyocytes to corroborate the potential benefits of PPARβ/δ activation under hyperglycemia conditions. The gene expression of the PPARβ/δ transcriptional targets

Table 2
Biochemical, biometric, echocardiographic and hemodynamic variables of wild-type male mice fed a standard diet supplemented with (CT) or without GW0742 (1 mg/kg/day, GW) for 8 weeks after the onset of diabetes. Diabetes was induced by intraperitoneal injection of streptozotocin (STZ; 50 mg/kg body weight) for five consecutive days. Mice serving as controls were given the same volume of sodium citrate 0.1 M pH 4.5.

	Group			
Parameter	CT	STZ	GW	STZ+GW
Glycemia (mg/dL)	138.1 ± 20.6	408.7 ± 114.9***	150.8 ± 14.4	410.2 ± 99.3$^{***,\&\&\&}$
Body weight (g)	31.0 ± 5.4	24.9 ± 2.9*	31.8 ± 3.9	27.0 ± 2.9$^{\&}$
Heart weight (mg)	141.5 ± 20.1	103.4 ± 11.5***	130.5 ± 23.5	126.8 ± 10.7$^{\#}$
HW/BW (mg/g)	4.5 ± 0.3	4.1 ± 0.2**	4.3 ± 0.4	4.4 ± 0.2$^{\#}$
HW/TL (mg/mm)	8.0 ± 0.8	6.3 ± 0.7***	7.9 ± 0.6	7.1 ± 0.6$^{**,\&\&,\#\#}$
EF (%)	57.8 ± 12.4	66.3 ± 12.0	57.5 ± 15.3	63.6 ± 12.9
FS (%)	26.2 ± 7.8	32.3 ± 8.9	26.5 ± 8.5	32.9 ± 9.0
IVSd (mm)	0.70 ± 0.25	1.05 ± 0.46	1.01 ± 0.30	0.94 ± 0.18
IVSs (mm)	0.83 ± 0.30	1.15 ± 0.43	1.33 ± 0.23	1.09 ± 0.15
PWTd (mm)	0.79 ± 0.25	0.95 ± 0.31	1.10 ± 0.41	1.03 ± 0.23
PWTs (mm)	0.83 ± 0.32	1.21 ± 0.53	1.15 ± 0.34	1.12 ± 0.27
LV EDD (mm)	3.46 ± 0.62	3.49 ± 0.77	3.70 ± 0.7	3.26 ± 0.6
LV ESD (mm)	2.57 ± 0.65	2.42 ± 0.74	2.65 ± 0.68	2.32 ± 0.73
Ao VTI (mm2)	5.15 ± 1.16	4.62 ± 1.62	3.70 ± 0.80	5.03 ± 1.42
Ao PV (mm/sec)	1.04 ± 0.37	1.39 ± 0.95	0.76 ± 0.11	0.95 ± 0.30
Systolic BP (mmHg)	119.7 ± 9.8	103.2 ± 31.2	114.3 ± 10.6	108.9 ± 11.5
Diastolic BP (mmHg)	56.7 ± 10.9	59.0 ± 20.8	51.9 ± 18.2	52.0 ± 10.7
Mean BP (mmHg)	77.3 ± 9.3	76.7 ± 17.1	77.2 ± 15.5	71.7 ± 7.3
Heart rate (bpm)	702 ± 46	617 ± 28**	688 ± 22	617 ± 47$^{**,\&}$

Data indicate median ± SD (n = 9–12 mice per group).
Abbreviations: BP, blood pressure; BW, body weight; HW, heart weight; TL, tibial length; EF, ejection fraction; FS, fractional shortening; IVSd, interventricular septal wall thickness at end-diastole; IVSs, interventricular septal wall thickness at end-systole; PWTd, left ventricular posterior wall thickness at end-diastole; PWTs, left ventricular posterior wall thickness at end-systole; LV EDD, left ventricular end-diastolic diameter; LV ESD, left ventricular end-systolic diameter; Ao VTI, aortic velocity time integral (aortic valve area); Ao PV, aorta peak velocity.
$^{*}P<0.05$, $^{**}P<0.01$ and $^{***}P<0.001$ vs. CT; $^{\&}P<0.05$, $^{\&\&}P<0.01$ and $^{\&\&\&}P<0.001$ vs. GW0742; $^{\#}P<0.05$, $^{\#\#}P<0.01$ and $^{\#\#\#}P<0.001$ vs. STZ.

ANGPTL4 and *PDK4* (pyruvate dehydrogenase kinase 4) were used to confirm the activation of this nuclear receptor by GW501516 (supplementary Fig. S4A). Exposure of cells to high glucose concentration for 72 h (HG, 50 mM) induced the expression of inflammation (*CCL2*, *IL6*, *IL10*, *TNF-α*) and fibrosis (*CCN2*, *COL1a1*, *MMP9*, *TGFB1*) markers compared to cells exposed to low glucose concentration (control, CT; 5.5 mM) (Fig. 6A). We also checked IκBα and p65 protein levels and, as expected, hyperglycemia downregulated IκBα and increased the p65 protein levels (Fig. 6B). FOS and JUN levels were also significantly higher in HG-treated cells (Fig. 6B). Addition of the PPARβ/δ agonist GW501516 to the media before exposing the cells to high glucose concentrations abrogated the increase in the expression of most of these genes, and prevented the rise in p65, FOS, and JUN protein levels (Fig. 6B). Assessment of DNA binding activity demonstrated that GW501516 treatment diminished the activity of p65/NF-κB and FOS/AP-1 transcriptional activity in cells exposed to high glucose levels (supplementary Fig. S4B). In our conditions, IκBα levels were not

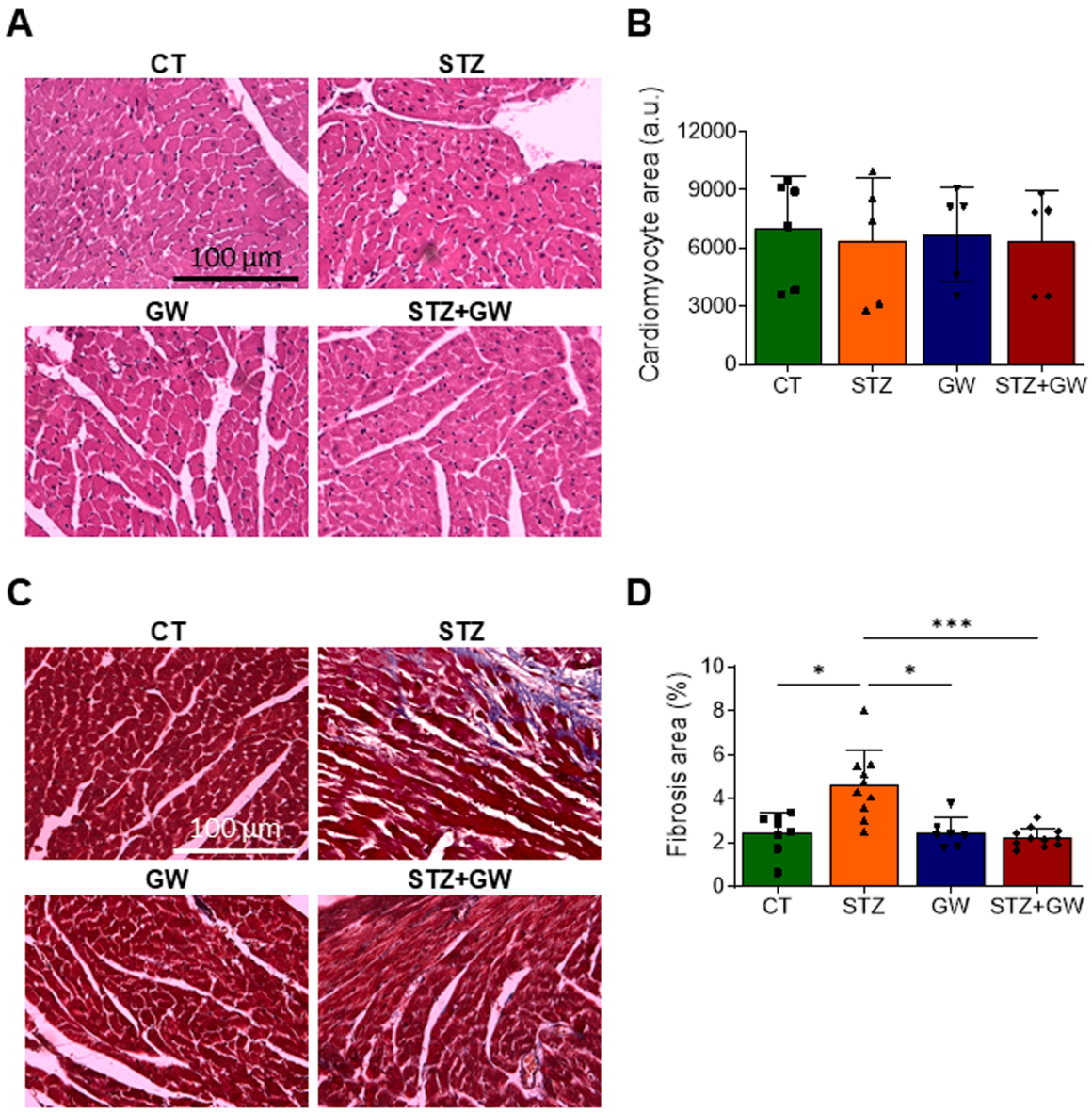

Fig. 4. The PPARβ/δ agonist GW0742 prevents myocardial collagen deposition in STZ-induced diabetic mice. Representative hematoxylin and eosin-stained micrographs (A) showing transverse sections from the left ventricle myocardium and quantification of cardiomyocyte cross-sectional areas (B) in diabetic mice (STZ) and their normoglycemic littermates (CT), treated with or without the PPARβ/δ agonist GW0742 (GW) for the last 16 weeks of diabetes. Representative images of Mason's trichrome staining (C) and quantification of fibrosis expressed as a percentage of control non-diabetic (CT) samples in the heart (D) of the same animal groups. Data are presented as the mean ± SD (n = 6–12 mice per group). $^{*}P < 0.05$, $^{**}P < 0.01$, $^{***}P < 0.001$.

normalized by the PPARβ/δ agonist GW501516. Similar to the results obtained *in vivo*, an elevation in some apoptotic markers (*BCL2L1*, *BAX/BCL2* ratio, Fig. 7A; BCL2, CHOP, and cleaved PARP1, Fig. 7B) was observed in hyperglycemic conditions, which was prevented after GW501516 treatment.

To confirm these results, we replicated some of these experiments in mouse atrial HL-1 cells and using another PPARβ/δ agonist, GW0742. The expression of *Angpl4* was used to confirm the effect of GW0742 on HL-1 cells (supplementary Fig. S5A). Hyperglycemia significantly induced the expression of inflammatory (*Il6*), fibrosis (*Col1a1*, *Mmp9*, *TGFB1*), apoptosis (*Ddit3*) and hypertrophic (*Nppb*) markers compared to cells exposed to low glucose concentration (supplementary Fig. S5A). Addition of GW0742 to the media before exposing the cells to high glucose concentrations abolished the increase in the expression of most of these genes.

Myocardial fibrosis involves the loss of cardiomyocytes, myocardial fibroblast activation and differentiation into myofibroblasts, and a reduction in angiogenesis [34]. To investigate to potential contributing role of cardiac fibroblast in the above-described anti-inflammatory and anti-fibrotic effects of PPARβ/δ agonists, we conducted an experiment with human cardiac fibroblasts (HCF) exposed to hyperglycemia, and in the presence or the absence of GW501516. As it is shown in Fig. 8A and B, high glucose treatment induced the expression of some genes related to inflammation (*CCL2*, *IL6*) and fibrosis (*CCN2*), but several others remained unaltered (*COL1a1*, *COL3a1*, *MMP2*, *MMP9*, *IL10*, *TGFB1*, and *TNF-α*). Even though HCF displayed higher *PPARD* gene expression than AC16 cells (supplementary Fig. S5B), coincubation of these cells with GW501516 only prevented the increase in *CCN2* induced by hyperglycemia, but had no effect on other genes (Fig. 8A and B). *PDK4* expression was measured to assess the activation of PPARβ/δ by GW501516 (supplementary Fig. S5C).

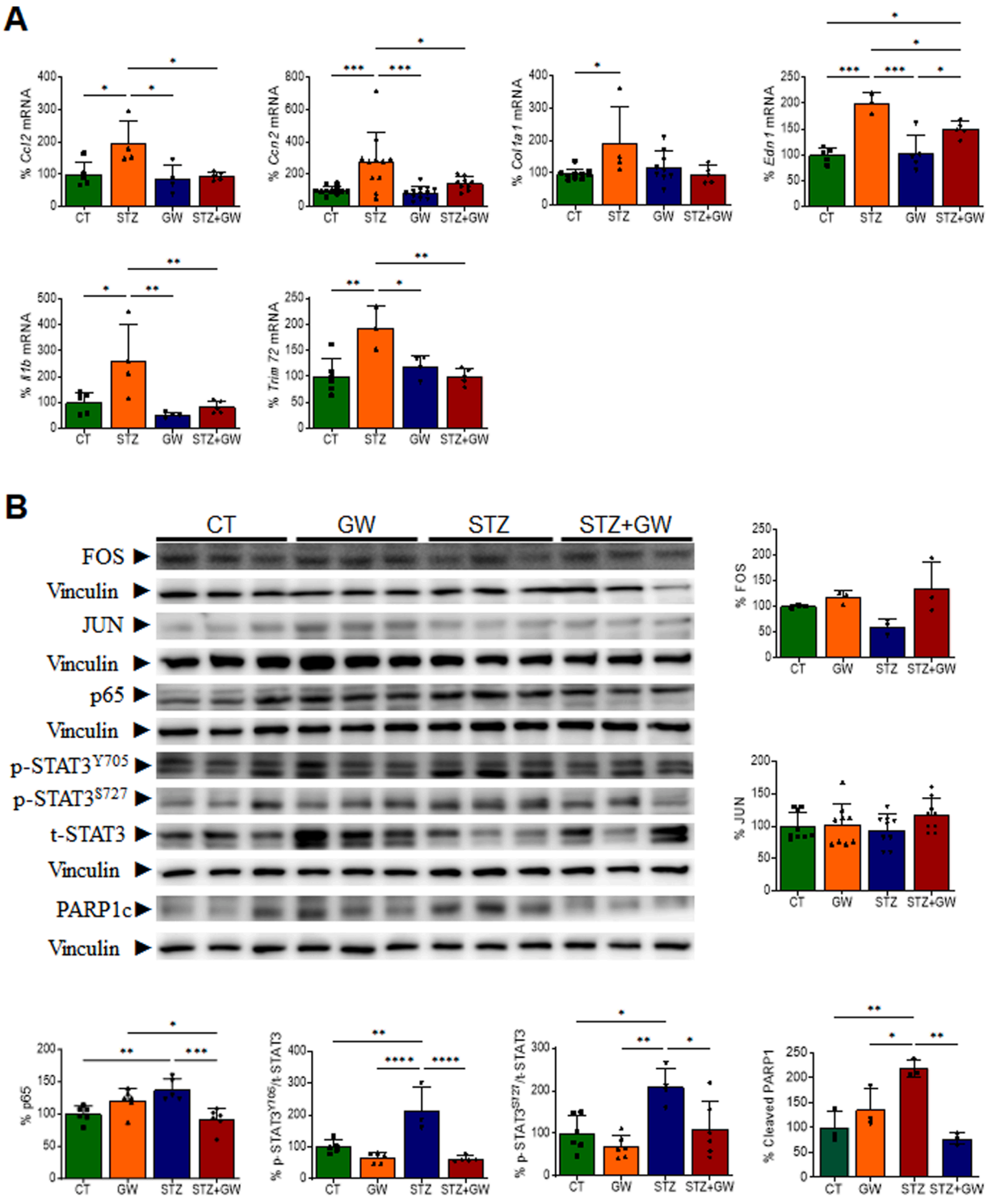

Fig. 5. PPARβ/δ activation downregulates inflammation and fibrosis during DCM in mice. A Relative quantification of the mRNA expression of *Ccl2*, *Ccn2*, *Col1a1*, *Edn1*, *Il1b*, and *Trim72* in diabetic mice (STZ) and their normoglycemic littermates (CT), treated with or without the PPARβ/δ agonist GW0742 (GW) for the last 16 weeks of diabetes. B Western blot analysis showing the protein levels of FOS, JUN, p65, p-STAT3^{Y705}/STAT3, p-STAT3^{S727}/STAT3, and PARP1c in the same animal groups. The graphs represent the quantification of adenine phosphoribosyl transferase (*Aprt*)-normalized mRNA levels (A) or the normalized quantification of protein levels (B) expressed as a percentage of the control samples. Data are presented as the mean ± SD (n = 6–12 mice per group). $^{*}P < 0.05$, $^{**}P < 0.01$, $^{***}P < 0.001$.

3.5. PPARβ/δ negatively correlates with collagen expression in the left ventricle of diabetic patients

Morphologic changes during DCM entail increased deposition of myocardial matrix extracellular proteins, above all type I and III collagens, which results in interstitial and perivascular fibrosis, reduces overall cardiac contractility, and leads to subsequent LV diastolic and systolic dysfunction in patients with type 1 and type 2 diabetes mellitus [35,36]. The etiology of this collagen accumulation is multifactorial, but the main cause of myocardial fibrosis is the overproduction and impaired degradation of collagen in both left and right ventricles [35]. Since PPARβ/δ activation has been previously demonstrated to inhibit

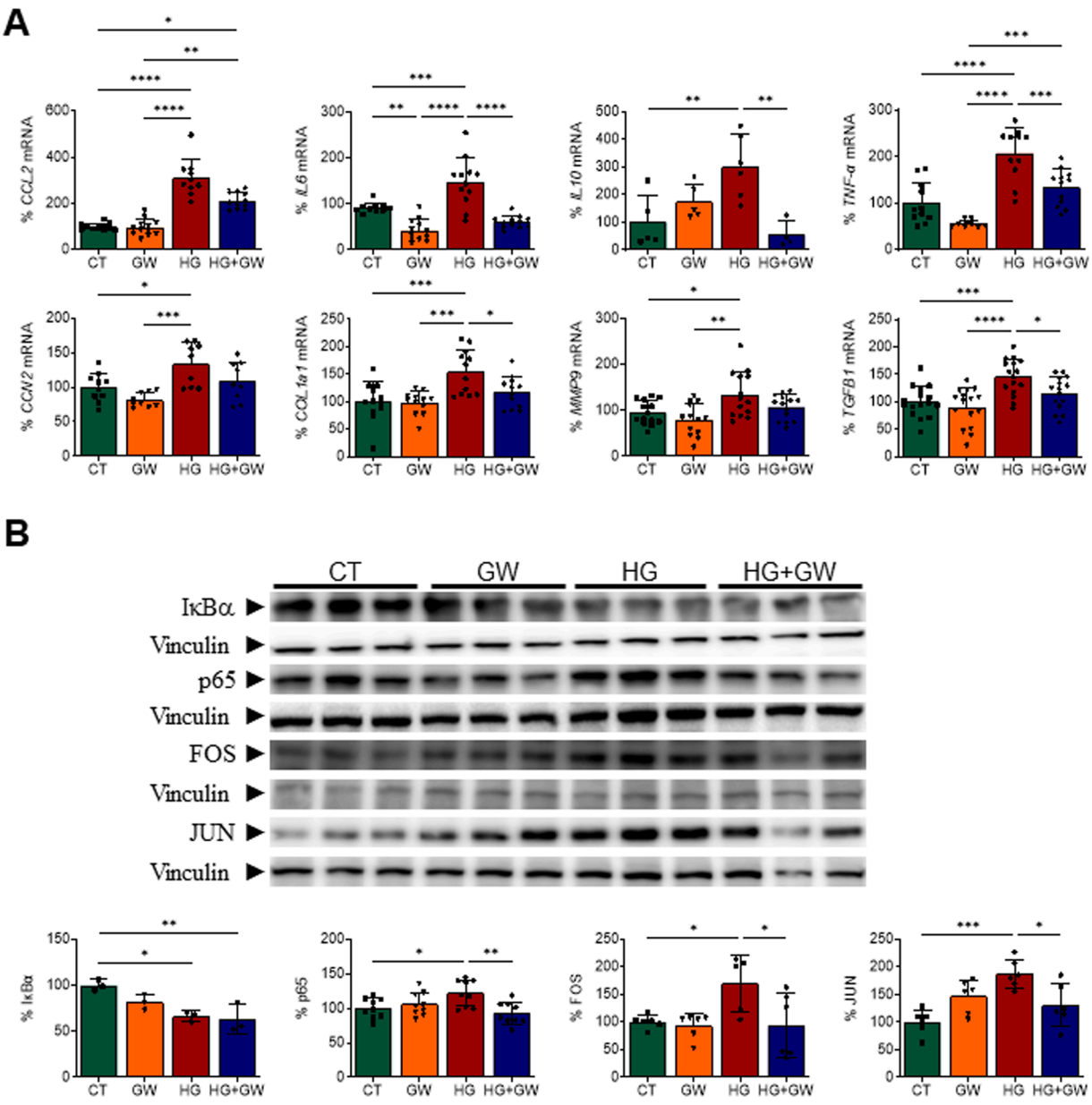

Fig. 6. PPARβ/δ activation downregulates inflammation and fibrosis in human cardiac cells. A Relative quantification of the mRNA expression of *CCL2*, *CCN2*, *COL1a1*, *IL6*, *IL10*, *MMP9*, *TGFB1*, and *TNF-α* in AC16 cells exposed to high glucose concentration for 72 h (HG, 50 mM) in the presence, or absence, of GW501516 (GW, 10 μM, added from 24 h before high glucose treatment). B Western blot analysis showing the protein levels of IκBα, FOS, JUN, and p65 in the same groups. The graphs represent the quantification of *TBP* (TATA-box binding protein)-normalized mRNA levels (A) or the normalized quantification of protein levels (B) expressed as a percentage of the control samples. Data are presented as the mean ± SD. $^{*}P < 0.05$, $^{**}P < 0.01$, $^{***}P < 0.001$.

angiotensin II-induced collagen type I expression, we next examined whether PPARβ/δ correlated with type I and III collagen levels in left ventricular myocardial biopsies obtained at surgery from diabetic patients. As it is shown in Fig. 8C, the relative expression of the PPARβ/δ gene (*PPARD*) negatively correlated with that of the profibrotic markers *COL1a1* (Pearson correlation coefficient r = −0.47, $P < 0.05$) and *COL3a1* (Pearson correlation coefficient r = −0.57, $P < 0.05$) in these patients.

3.6. MAPK inhibition might account for the beneficial effects of PPARβ/δ activation in AC16 cells exposed to hyperglycemia

Next, we sought to determine the molecular mechanism by which PPARβ/δ activation might inhibit inflammation and fibrosis within the context of DCM. It has been reported that PPARα may increase the levels of NF-κB inhibitor α (IκBα) in cardiac cells through the binding to a peroxisome proliferator response element (PPRE) located within the promoter region of its gene (*NFKBIA*) [37]. IκBα forms a cytoplasmic inactive complex with the p65/p50 heterodimer and, thus, inhibits NF-κB signaling. In our conditions, GW501516 treatment of AC16 cells did not transcriptionally induce *NFKBIA* (supplementary Fig. S6A) or increase the protein levels of IκBα (Fig. 6B), regardless the presence of hyperglycemia. Although short term induction of IκBα expression by GW501516 cannot be disregarded, our results seem to rule out this mechanism.

PPARs may also negatively regulate the activity of other transcription factors, including NF-κB and AP-1, through PPRE-independent pathways in a transrepression process [38]. Transrepression includes three main mechanisms that account for most of the anti-inflammatory effects of PPARs [6,38]. The first one arises from competition for shared

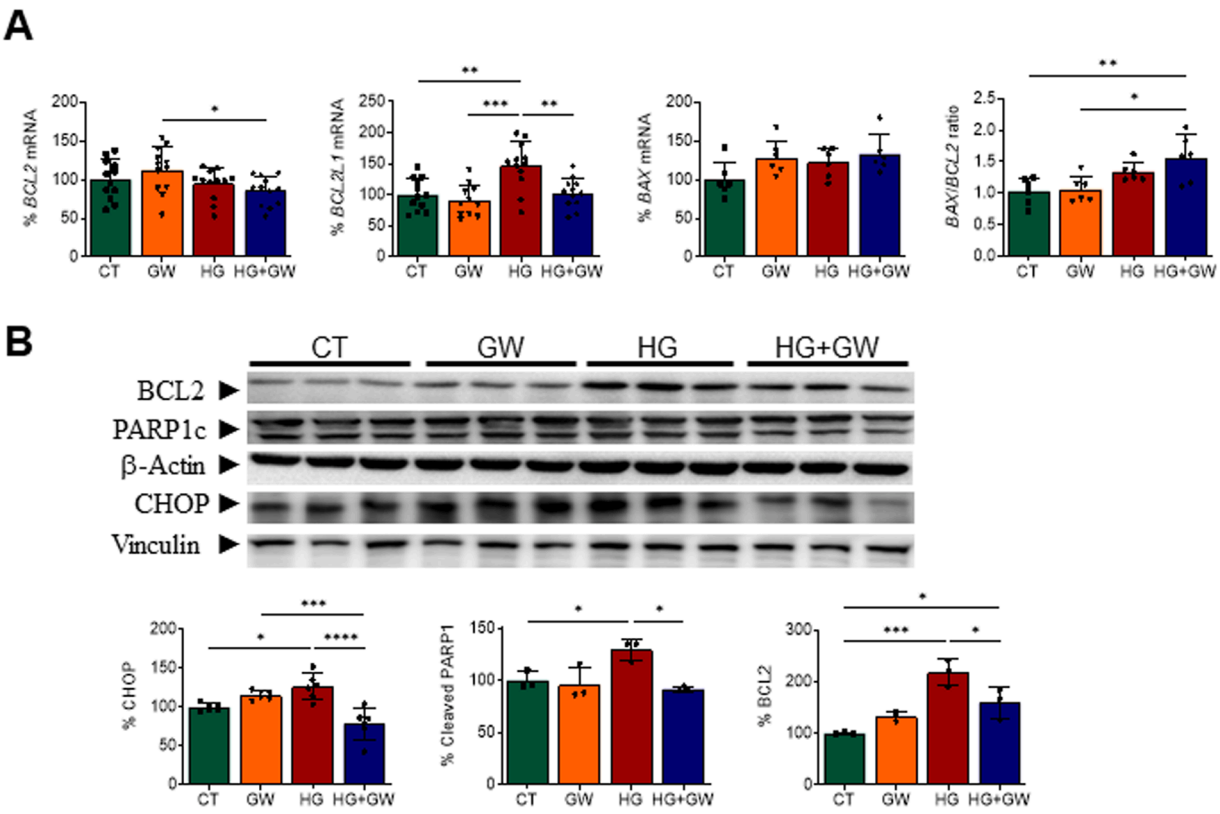

Fig. 7. Effect of hyperglycemia and GW501516 on several apoptotic markers in human cardiac AC16 cells. A Relative quantification of the mRNA expression of *BCL2*, *BCL2L1*, *BAX*, and the *BAX/BCL2* ratio in AC16 cells exposed to high glucose concentration for 72 h (HG, 50 mM) in the presence, or absence, of GW501516 (GW, 10 μM, added from 24 h before high glucose treatment). B Western blot analysis shows the protein levels of CHOP, PARP1, and BCL2 in the same groups. The graphs represent the quantification of *TBP* (TATA-box binding protein)-normalized mRNA levels (A) or the normalized quantification of protein levels (B) expressed as a percentage of the control samples. Data are presented as the mean ± SD. $^{*}P < 0.05$, $^{**}P < 0.01$, $^{***}P < 0.001$.

coactivators; as a consequence, PPAR activation will result in lesser activation of other transcription factors that use the same coactivators. The second one occurs through physical interaction between transcription factors, which hinders their binding to the corresponding response elements in the promoter region and, thereby, causes a functional cross-inhibition of their transcriptional activity. The last mechanism relies on the ability of activated PPARs to inhibit the phosphorylation and subsequent activation of mitogen-activated protein kinases (MAPK), thus preventing the activation of downstream transcription factors.

It has been previously reported that agonist-mediated PPARβ/δ activation inhibits NF-κB in cultured neonatal rat cardiomyocytes and embryonic rat heart-derived H9c2 cells by promoting a protein-protein interaction between the p65 subunit of NF-κB and PPARβ/δ [39,40]. However, coimmunoprecipitation studies revealed that GW501516 or hyperglycemia did not modify the physical interaction between p65 or FOS and PPARβ/δ in human cardiac AC16 cells, thus making this mechanism unlikely to explain our results. Notably, we had previously reported that PPARβ/δ activation by GW501516 enhanced the physical interaction between PPARβ/δ and p65 in the heart of mice fed a high-fat diet and in palmitate-treated AC16 cells [41]. In that study, we demonstrated that PPARβ/δ activation abrogated the pro-inflammatory profile through both AMPK- (AMP-activated protein kinase) and PPARβ/δ-dependent mechanisms. Since activation of AMPK may block the NF-κB signaling pathway through the blockade of IκB kinase activity [42], it might be possible that GW501516 was blocking the pro-inflammatory and pro-fibrotic pathways through AMPK-dependent mechanisms. Another study demonstrated that AMPK also inhibits STAT3 in hepatocytes [43]. However, in the current study no changes in AMPK activity were detected neither *in vivo* nor *in vitro* (supplementary Fig. S6B and C), suggesting the participation of alternative mechanisms.

Next, we checked MAPK signaling pathways, that is, extracellular signal-regulated kinase 1/2 (ERK1/2), c-Jun N-terminal protein kinase (JNK) and p38 MAP kinase. Western-blot analyses revealed that all three MAPK were phosphorylated, and thus activated, after hyperglycemia treatment in AC16 cells, while GW501516 pretreatment prevented these changes (Fig. 9A). Finally, to confirm that these MAPK kinases were involved in the harmful effects posed by hyperglycemia in AC16 cells, cells were incubated with high concentrations of glucose in the presence or absence of selective inhibitors for ERK1/2 (U0126), JNK (SP600125) and p38 (SB202190) MAPK. Inhibition of ERK1/2 activity prevented the increase in *IL6*, *IL10*, *TGFB1* and *TNF-α* mRNA levels induced by hyperglycemia, while JNK and p38 MAPK inhibition abolished the effects on all these genes except *IL10* (Fig. 9B). These results reinforce the idea that PPARβ/δ activation protects cardiac cells by inhibiting MAPK activity, and also indicate that these kinases play complementary, but slightly different roles, during DCM.

4. Discussion

PPARβ/δ is a key metabolic regulator that is dysregulated in the heart during diabetes. This nuclear receptor displays potential anti-diabetic effects due to its ability to attenuate inflammation and subsequent cardiac remodeling and dysfunction during cardiac disease. According to this, cardiomyocyte-restricted deletion of PPARβ/δ results in cardiac dysfunction and steatosis of the heart [15], while cardiomyopathy induced by hyperglycemia in STZ-treated rats is associated with a marked decrease in PPARβ/δ expression [23] and increased myocardial inflammation [30]. In the present study, we report that PPARβ/δ plays a protective role during DCM, and that its activation prevents some of the deleterious effects of diabetes in the heart.

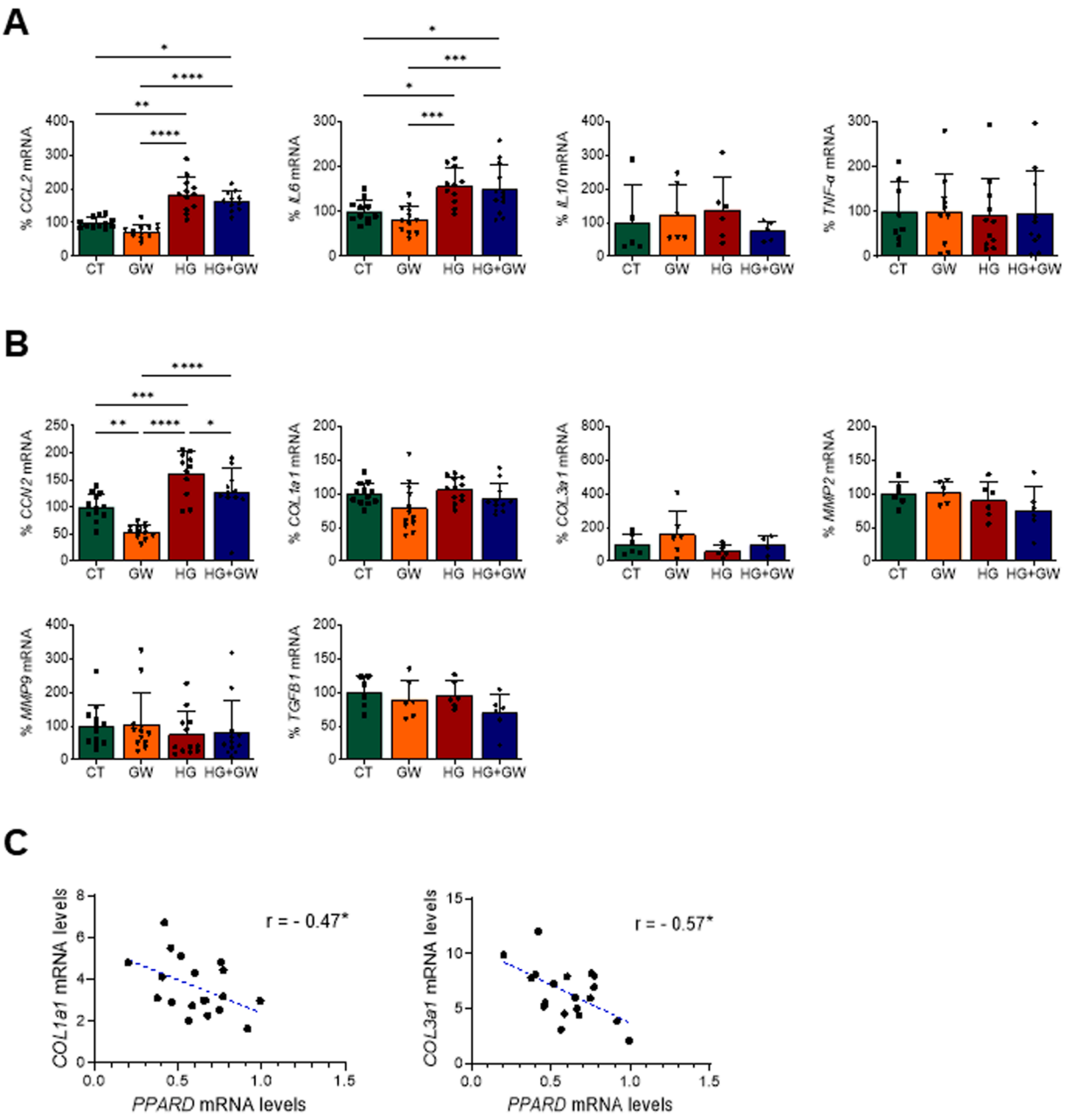

Fig. 8. Effects of PPARβ/δ activation on human cardiac fibroblasts. Relative quantification of the mRNA expression of (A) *CCL2*, *IL6*, *IL10*, and *TNF-α*; or (B) *CCN2*, *COL1a1*, *COL3a1*, *MMP2*, *MMP9*, and *TGFB1* in human cardiac fibroblasts exposed to high glucose concentration for 72 h (HG, 50 mM) in the presence, or absence, of GW501516 (GW, 10 μM, added from 24 h before high glucose treatment). The graphs represent the quantification of *TBP* (TATA-box binding protein)-normalized mRNA levels expressed as a percentage of the control samples. Data are presented as the mean ± SD. C Linear regression and Pearson's correlation analysis between *PPARD* and *COL1a1* or *COL3a1* gene expression in intraoperative left ventricular myocardial biopsies obtained from a cohort of 19 diabetic patients with severe aortic stenosis. The relative transcript levels of the target genes, in arbitrary units, were used to calculate the Pearson correlation coefficients (r). $^{*}P < 0.05$, $P < 0.01$, $^{***}P < 0.001$.

Like others, we did not observe cardiac dysfunction, nor significant cardiac hypertrophy, at 6 months after STZ-induced diabetes in WT mice [25]. However, other previous studies reported that these parameters are modified after inducing diabetes in male mice [29,30,44]. The different genetic background of the mouse strains used might account for these discrepancies. In fact, the lack of cardiac diastolic and systolic dysfunction in diabetic male mice has been described in a study that compared the effect of gender on STZ-induced DCM. According to this study, when systolic dysfunction was already evident in female diabetic mice, cardiac dysfunction had not yet emerged in males [25]. In our study, echocardiographic analysis suggested the occurrence of incipient dilated cardiomyopathy, without systolic dysfunction, in WT diabetic and PPARβ/δ KO mice (both diabetic and non-diabetic), and assessment of anatomic structure demonstrated a cardiac wall thickening only in KO mice, regardless of whether they were diabetic or not. Although other studies have reported a significant reduction in septal and posterior wall thicknesses in STZ-induced diabetic murine models [12,25], we did not find significant anatomic changes in the heart geometry of WT diabetic mice. Strikingly, the thickening of cardiac walls was only reduced after induction of diabetes in PPARβ/δ KO mice. These findings suggest the existence of cardiac wall thickening in PPARβ/δ KO mice. In contrast, STZ-induced diabetes would cause wall thinning and chamber dilation in the absence of PPARβ/δ.

The myocardium responds to numerous pathological stimuli by

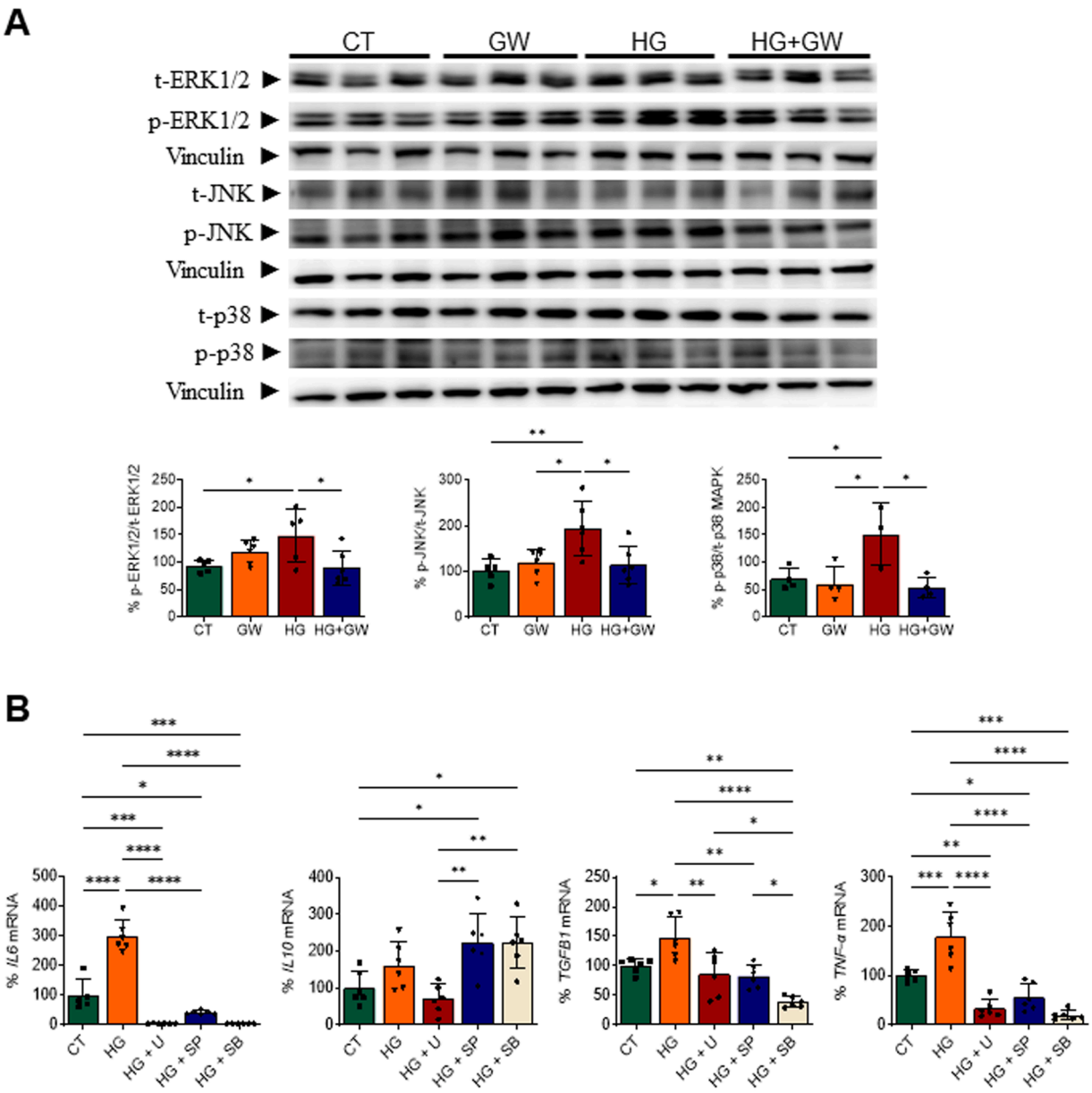

Fig. 9. PPARβ/δ activation prevents the deleterious effects of hyperglycemia by inhibiting MAPK activity. A Western blot analysis showing the protein levels of p-ERK1/2/ERK1/2, p-JNK/JNK, and p-p38/p38 MAPK in AC16 cells exposed to high glucose concentration for 72 h (HG, 50 mM) in the presence, or absence, of GW501516 (GW, 10 μM, added from 24 h before high glucose treatment). B Relative quantification of the mRNA expression of *IL6*, *IL10*, *TGFB1*, and *TNF-α* in AC16 cells exposed to high glucose concentration for 72 h (HG, 50 mM) in the presence, or absence, of selective ERK1/2 (U0126), JNK (SP600125), and p38 (SB202190) MAPK (10 μM each, added from 24 h before high glucose treatment). The graphs represent the quantification of *TBP* (TATA-box binding protein)-normalized mRNA levels (B) or the normalized quantification of protein levels (A) expressed as a percentage of the control samples. Data are presented as the mean ± SD. $^{*}P < 0.05$, $^{**}P < 0.01$, $^{***}P < 0.001$, $^{****}P < 0.0001$.

expressing and secreting several pro-inflammatory cytokines and chemokines, contributing to cardiac remodeling and malfunction and, thereby, speeding up heart failure progression [45]. Myocardial fibrosis is a characteristic hallmark of DCM [30,32,44,46]. On cardiac stress, myofibroblasts begin to produce collagen, which, after deposition and cross-linking, contributes to myocardial fibrosis and dysfunction, be it diastolic or combined. Masson's trichrome staining revealed significant collagen accumulation in the diabetic mice, pointing to the development of cardiac fibrosis, particularly in those animals with PPARβ/δ suppression. Therefore, exacerbated myocardial fibrosis in PPARβ/δ KO mice would not account for the entirety of the cardiac dysfunction described above, as, in fact, has already been demonstrated in other studies [25]. At the molecular level, the upsurge of fibrosis correlated with the increased gene expression of several pro-inflammatory and pro-fibrotic markers previously linked to DCM. The occurrence of inflammation and fibrosis has already been reported in the heart of PPARβ/δ KO mice [41] and diabetic mice [6,8,9,29,30,44,47]. Still, here we observed a synergistic effect of combining both PPARβ/δ deletion and diabetes for several of these markers. For instance, *Il1b* has been related to DCM-induced pyroptosis in *in vitro* studies [48], whereas *Il10* is an anti-inflammatory cytokine transcriptionally regulated by STATs that is increased in the heart of diabetic mice [49]. In contrast, Thomas et al. [29] observed no increase in *Il1b* or *Tnf-α* expression in the heart after 24 weeks of diabetes induction, thereby concluding that these mediators were not related to cardiac dysfunction at that time of diabetes evolution. *Lgals3* encodes for a β-galactoside-binding lectin potentially useful as a biomarker in heart failure with proinflammatory activity [50]. LGALS3, by promoting the expression of several mediators

in the heart, including *Ccn2* and *Col1a1*, is required for diabetogenesis in the multiple low-dose STZ-induced diabetic mice model [51]. *Trim72* encodes for a striated muscle-specific E3 ligase abundantly expressed in the myocardium that has been robustly linked to DCM, probably due to its ability to impair insulin signaling [52] and to induce excessive deposition of extracellular matrix and fibrosis [53,54]. Of note, to carry out such effects, TRIM72 requires the activation of STAT3 in cardiac fibroblasts. Despite TRIM72 having also been linked to atrial fibrosis through the activation of the TGFβ pathway [53], we did not find differences in TGFβ levels at the transcriptional level. We also observed an increase in the mRNA levels of *Nr1d1* (Rev-Erbα), a nuclear receptor induced after myocardial infarction that aims to suppress excess inflammatory response and fibrosis after myocardial infarction [55,56]. Interestingly, NR1D1 also modulates glucose and lipid metabolism in cardiac cells [55].

Regarding the relative role of the two main cell types involved in cardiac fibrosis and remodeling, namely cardiomyocytes and fibroblasts, we have demonstrated that the treatment with PPARβ/δ agonists exerted beneficial effects on both cell types. Thus, GW501516 prevented the increase in pro-inflammatory and pro-fibrotic markers induced by hyperglycemia in human cardiomyocytes and, to a lesser extent, also in cardiac fibroblasts. This might explain the strong beneficial effect displayed by GW0742 *in vivo*. In fact, Teunissen et al. already demonstrated that activation of PPARβ/δ inhibited cardiac fibroblast proliferation and its transdifferentiation into myofibroblasts, thus reducing fibrosis [57], whereas Liu and collaborators established an interplay between TGFβ and PPARβ/δ in regulating cardiac fibroblast activation and cardiac fibrosis [58]. The latter study also showed that GW501516 antagonized TGFβ signaling and cardiac fibroblast activation. Diabetes-related cardiac fibrosis is modulated by increasing level of TGFβ released by cardiomyocyte and non-cardiomyocyte cells, including fibroblasts, but also vascular smooth muscle cells, endothelial cells, mast cells, macrophages, and dendritic cells [34,59]. In fact, despite myofibroblast activation is a main effector in cardiac fibrosis, its activation is brought about through a cascade of growth factors (TGFβ), inflammatory cytokines and chemokines, ROS, metallopeptidases, and endothelin 1 secreted by both cardiomyocytes and non-cardiomyocyte cells [34,60]. Not surprisingly, long-term hyperglycemia increases intracellular cardiomyocyte cytokines, which play a pivotal role in extracellular matrix overproduction [61]. Anyhow, the extent of fibroblast response to hyperglycemia in our human model was incomplete, since no increase in the expression of collagens, *MMP2*, *MMP9*, or *TGFB1* was observed. These results point to cardiomyocytes as the most important cell type in the beneficial effects of PPARβ/δ activation observed during DCM in our models.

As previously reported [41], the protein levels of the p65 subunit of NF-κB and the activity of STAT3 were up-regulated in the heart of PPARβ/δ KO mice. Hyperglycemia had no effect on NF-κB since, unlike a previous study using the same model [29], we did not observe increased levels of p65 protein. STAT3, which was particularly activated in those mice that were also diabetic, is a pro-inflammatory transcription factor that also participates in the pathophysiological development and progression of DCM, where it regulates cardiac remodeling and processes related to inflammation and cell death [22,62,63]. In fact, STAT3 may not only activate NF-κB, but it is also required to maintain NF-κB activity [22], which means controlling cardiac inflammation [63]. STAT3 is activated in cardiac cells after the induction of diabetes with STZ in mice and rats, and also in cultured primary rat cardiac fibroblasts and H9c2 cells exposed to hyperglycemia [64–66]. Here we also depict that the protein levels of FOS and JUN subunits of AP-1 were increased in the hearts of KO and diabetic mice. AP-1 is a heterodimeric transcription factor composed of members belonging to the JUN, FOS, activating transcription factors (ATFs) and JUN-dimerization partner families. Through stimulating its target genes, including *Ccn2*, *Col1a1*, and *Mmp9*, AP-1 causes changes in the extracellular matrix, which eventually lead to cardiac fibrosis, decreased contractility, and heart failure [45,67]. Overall, these results indicate that NF-κB and AP-1 may favor the development of a pro-inflammatory and pro-fibrotic phenotype during DCM in these mice.

PPARβ/δ mRNA and protein levels are reduced in H9c2 rat myoblasts and neonatal rat cardiomyocytes exposed to hyperglycemia, and also in the heart of STZ-induced diabetic rats [23,68]. Still, we did not observe a downregulation in the expression of this transcription factor in our models. The reasons for this discrepancy are unknown, but could arise from species-specific differences or the distinct time of diabetes evolution and the different methods used for diabetes induction *in vivo*. Despite this, our study demonstrates a protective effect of PPARβ/δ during DCM, since treatment of diabetic mice with a selective agonist, GW0742, totally or partially prevented most of the harmful effects that hyperglycemia posed on the heart. PPARβ/δ activation prevented fibrosis and partially abolished the pro-inflammatory and pro-fibrotic responses characteristic of this type 1 diabetes model. Noticeably, this compound had no effect in non-diabetic animals. It has already been reported that PPARβ/δ activation may prevent hyperglycemia-induced fibrosis, which is brought about by STAT3 upregulation [69], and may suppress inflammation in the kidney of STZ-induced diabetic mice [24]. Similarly, another PPARβ/δ agonist, L-165041, prevented the increase of some pro-inflammatory markers observed in the serum [70] and cardiac tissue [30,44] of diabetic mice. Treatment with PPARβ/δ agonists has been capable of inhibiting NF-κB activation and subsequent inflammation induced in the heart by several stimuli, including phenylephrine, lipopolysaccharide, the saturated fatty acid palmitate, or a high-fat diet [15,41]. We also demonstrate here the protective effects of PPARβ/δ activation under hyperglycemia conditions *in vitro* in a mouse cardiac muscle cell line, HL-1, in human cardiac fibroblasts, and in a cardiac cell line of human origin, AC16. Treatment of these cells with GW0742 or GW501516 abrogated the increase in the expression of pro-inflammatory and pro-fibrotic genes caused by hyperglycemia, and prevented the rise in p65, FOS and JUN protein levels and the DNA binding activity of NF-κB and AP-1. This is relevant, since opposite and contradictory results have often been encountered when outcomes obtained with murine models have been extrapolated to humans, especially taking into account that PPARs are expressed at lower levels in human cells than in murine cells [71], and that their target genes are also differentially regulated among species [41,72].

Cardiomyocyte hypertrophy is a very complex process characterized by an increase in cell size and protein synthesis. Contradictory results regarding cardiomyocyte size have been found in studies with diabetic patients and animal models, in which both myocyte hypertrophy and atrophy have been observed [10]. Indeed, postmortem histological studies have revealed the occurrence of hypertrophic cardiomyocytes mixed with atrophic ones in DCM [73]. Other authors have reported morphological hypertrophy accompanied by the upregulation of molecular hypertrophy markers in STZ-induced diabetic rats and mice at 1, 3, and 6 months post-diabetes [29,30,44,46]. Likewise, increased expression of hypertrophic signals and cell hypertrophy has been observed in H9c2 myoblasts exposed to hyperglycemia, which is prevented by GW0742 pre-treatment [68]. In our study, although the expression of some molecular markers of cardiac hypertrophy (*Nppb*, *Myh7*) was increased in diabetic mice, no differences in the average cross-sectional diameter of cardiomyocytes were observed. Even the ratio of HW/TL was diminished in diabetic mice, particularly in those lacking the PPARβ/δ gene, thus pointing to some degree of atrophy. Several reasons may account for the lack of cell size variation in the presence of changes in the expression of pro-hypertrophic markers. For example, the increased expression of pro-hypertrophic markers might occur as an early adaptive response to stress, so the process of cardiomyocyte enlargement might be delayed or incomplete. Alternatively, the observed alterations in metabolism and the microenvironment of the cardiomyocytes, including changes in the composition, size and structure of the extracellular matrix, could impact their growth and development and, thus, influence cardiomyocyte hypertrophy. GW0742 treatment partially prevented the decrease in the HW/TL ratio observed

in diabetic mice but had no effect on the expression of genes related to cardiac hypertrophy, thus ruling out the effect of PPARβ/δ in cardiac cell size. These conflicting results might be due to the utilization of different procedures for diabetes induction, the diverse mouse strains, or even the various treatment periods after the onset of diabetes.

Cardiac atrophy during DCM could be attributed to the loss of cardiomyocytes [12], since we observed that some apoptotic markers were induced in STZ-treated mice. Activation of PPARβ/δ both *in vivo* and *in vitro* prevented the increase in some, but not all, of these molecular markers, thus suggesting the involvement of other pathways besides this nuclear receptor. Cardiomyocytes rarely proliferate within the adult heart, and thus, their loss due to apoptosis plays an essential pathogenic role during DCM [38,74]. In any case, the occurrence of apoptosis in the heart at late stages of diabetes is not completely established, as some studies report apoptosis, but others do not [12,32,44]. The transcription factor CHOP, which was induced during DCM, triggers the intrinsic apoptotic pathway by modulating the expression of the BCL2-family of proteins, increasing the mitochondrial outer membrane permeabilization and leading to the activation of the caspase cascade [75]. *Il1b*, which was also upregulated in STZ-treated mice and completely reversed after GW0742 treatment, has been involved in the apoptosis of cardiomyocytes and fibrosis in response to diabetes, through the induction of CHOP and MMPs, respectively [76]. On the other hand, CHOP also modulates apoptosis by up-regulating the expression of *Trib3* [30,75]. Even though the role of TRIB3 in apoptosis is still controversial, there is some consensus that it is partly responsible for cardiac cell death during diabetes as a result of sustained ER stress [5,77,78]. In rats with DCM, its mRNA and protein levels are increased, and silencing of *Trib3* ameliorates metabolic disturbances, inflammation, and fibrosis, among others [30]. Chronic ER stress activates NF-κB and other pro-apoptotic pathways [5,79], and both CHOP/*Ddit3* and *Trib3*, regarded as ER stress markers, were upregulated in STZ-induced diabetic mice, particularly in mice with PPARβ/δ suppression. During DCM, caspases cleave PARP1, inactivating its DNA repair function and contributing to cardiac complications through combining inflammation, oxidative stress, and fibrosis mechanisms, besides apoptosis [80]. BCL2 and BCL2L1 are considered anti-apoptotic factors, and the ratio of BAX to BCL2 (or BCL2L1) is often measured to assess the apoptotic state of cardiomyocytes in diabetes. However, some studies suggest that BCL2 and BCL2L1 may reactively increase to counteract the adverse effects of hyperglycemia on the myocardium [81]. The potential role of oxidative stress in inducing apoptosis has not been explored in the present work because there are several studies demonstrating its involvement in apoptotic cell death in STZ-induced diabetic cardiomyopathy [29], and GW0742 has already been shown to attenuate the increase in ROS caused by hyperglycemia exposure of H9c2 cells [68]. PPARβ/δ activation prevents oxidative stress-induced apoptosis in cardiac cells by several mechanisms, including the expression of anti-oxidative enzymes or by stopping the increase in the expression of MMPs [38].

Although we cannot exclude the competition for limited amounts of shared coactivators [38], the transrepression mechanism responsible for the beneficial effects of PPARβ/δ activation in our DCM models involves, at least in part, the inhibition of MAPK. Thus, ERK1/2, JNK, and p38 MAPK, known to be involved in the pathogenesis of DCM-associated fibrosis and inflammation [82–84], were all activated in the presence of hyperglycemia, while GW501516 prevented their activation. Moreover, blocking these kinases by selective inhibitors prevented inflammation and fibrosis in these cells. In support for the key role of MAPK in myocardial fibrosis, several studies have shown that they are overactivated during remodeling in heart failure and cardiac hypertrophy after myocardial infarction [85,86]. Further, the blockade of ERK1/2, JNK, or p38 MAPKs activity with small chemical inhibitors is sufficient to prevent fibrosis in the heart [87,88], the liver [89], the lung [90–92], the kidney [93,94], and even the skeletal muscle [95], thus pointing to that their inhibition might emerge as a potential intervention mechanism for treating fibrosis-related deleterious conditions in the heart. Likewise, previous works have shown that excess ROS production, hyperglycemia, and high circulating levels of lipids hasten inflammation, fibrosis, and cardiomyocyte apoptosis in DCM through the phosphorylation and subsequent activation of MAPKs and their downstream targets NF-κB and AP-1 [76,96–101]. Not surprisingly, pharmacological inhibition or genetic suppression of these MAPKs reduces DCM caused by type 1 diabetes in rodents [99]. More recent studies show that STAT3 and ERK1/2 are activated during diabetes in the heart, and that inhibition of STAT3 attenuates cardiomyopathy in STZ-induced type 1 diabetes [62,63,84]. Similar to our data, a recent study performed in primary rat astrocytes has demonstrated that GW501516 significantly decreases the lipopolysaccharide-mediated activity of ERK1/2, p38, and JNK MAPK, but does not influence their activity in naive cells [102]. This inhibition might account for the more effective anti-inflammatory effects of PPARβ/δ ligands compared with PPARα and PPARγ ligands.

5. Conclusion

The present study identifies PPARβ/δ as an essential factor contributing to the pathogenesis of diabetic cardiomyopathy. Despite PPARβ/δ has been postulated as a potential target in the treatment of obesity and the insulin resistance status, no selective PPARβ/δ agonists have yet been approved for human use. Although we did not unequivocally demonstrate that the PPARβ/δ agonists used in this study specifically activated this nuclear receptor, our results suggest that its activation might serve as a therapeutic target for preventing or treating diabetic cardiomyopathy due to its anti-inflammatory and anti-fibrotic effects. Inhibition of stress MAPKs by PPARβ/δ seems to account for its protective effects on the heart.

Funding

This work was partly supported by the grants PID2021-122116OB-I00 (M.V.-C. and X.P.), funded by MICIU/AEI/10.13039/501100011033 and "ERDF, A Way of Making Europe", the "Fundació La Marató de TV3" to M.V-C, and FIS PI21/00084 (Carlos III Health Institute) (J.F.N.). CIBER in Diabetes and Associated Metabolic Diseases (CIBERDEM), CIBER of Rare Diseases (CIBERER), and CIBER in Cardiovascular Diseases (CIBERCV) are Carlos III Health Institute projects. Support was also received from the CERCA Programme/Generalitat.

CRediT authorship contribution statement

Brenda Valenzuela-Alcaraz: Investigation. **Fátima Crispi:** Investigation. **Javier Pizarro-Delgado:** Methodology, Investigation. **Emma Barroso:** Investigation. **J. Francisco Nistal:** Writing – review & editing, Project administration, Methodology, Investigation, Funding acquisition, Formal analysis, Conceptualization. **María A. Hurlé:** Investigation. **Raquel García:** Investigation. **Adel Rostami:** Methodology, Investigation, Formal analysis. **Xavier Palomer:** Writing – review & editing, Writing – original draft, Methodology, Investigation, Funding acquisition, Formal analysis, Data curation, Conceptualization. **Walter Wahli:** Writing – review & editing, Investigation. **Manuel Vazquez-Carrera:** Writing – review & editing, Writing – original draft, Validation, Supervision, Resources, Project administration, Methodology, Investigation, Funding acquisition, Formal analysis, Data curation, Conceptualization.

Declaration of Competing Interest

none.

Acknowledgements

We want to thank the Language Services of the University of Barcelona for revising the manuscript.

Appendix A. Supporting information

Supplementary data associated with this article can be found in the online version at doi:10.1016/j.phrs.2024.107515.

Data availability

Data will be made available on request.

References

[1] M.M. Redfield, S.J. Jacobsen, J.C. Burnett Jr., D.W. Mahoney, K.R. Bailey, R. J. Rodeheffer, Burden of systolic and diastolic ventricular dysfunction in the community: appreciating the scope of the heart failure epidemic, JAMA 289 (2) (2003) 194–202.

[2] I.S. Thrainsdottir, T. Aspelund, G. Thorgeirsson, V. Gudnason, T. Hardarson, K. Malmberg, G. Sigurdsson, L. Ryden, The association between glucose abnormalities and heart failure in the population-based Reykjavik study, Diabetes Care 28 (3) (2005) 612–616.

[3] W.S. Lee, J. Kim, Diabetic cardiomyopathy: where we are and where we are going, Korean J. Intern Med 32 (3) (2017) 404–421.

[4] R. Retnakaran, B. Zinman, Type 1 diabetes, hyperglycaemia, and the heart, Lancet 371 (9626) (2008) 1790–1799.

[5] X. Palomer, J. Pizarro-Delgado, M. Vazquez-Carrera, Emerging actors in diabetic cardiomyopathy: heartbreaker biomarkers or therapeutic targets? Trends Pharm. Sci. 39 (5) (2018) 452–467.

[6] X. Palomer, L. Salvado, E. Barroso, M. Vazquez-Carrera, An overview of the crosstalk between inflammatory processes and metabolic dysregulation during diabetic cardiomyopathy, Int. J. Cardiol. 168 (4) (2013) 3160–3172.

[7] L.J. Rijzewijk, R.W. van der Meer, J.W. Smit, M. Diamant, J.J. Bax, S. Hammer, J. A. Romijn, A. de Roos, H.J. Lamb, Myocardial steatosis is an independent predictor of diastolic dysfunction in type 2 diabetes mellitus, J. Am. Coll. Cardiol. 52 (22) (2008) 1793–1799.

[8] O. Lorenzo, B. Picatoste, S. Ares-Carrasco, E. Ramirez, J. Egido, J. Tunon, Potential role of nuclear factor kappaB in diabetic cardiomyopathy, Mediat. Inflamm. 2011 (2011) 652097.

[9] Z. Pan, X. Sun, H. Shan, N. Wang, J. Wang, J. Ren, S. Feng, L. Xie, C. Lu, Y. Yuan, Y. Zhang, Y. Wang, Y. Lu, B. Yang, MicroRNA-101 inhibited postinfarct cardiac fibrosis and improved left ventricular compliance via the FBJ osteosarcoma oncogene/transforming growth factor-beta1 pathway, Circulation 126 (7) (2012) 840–850.

[10] O. Asghar, A. Al-Sunni, K. Khavandi, A. Khavandi, S. Withers, A. Greenstein, A. M. Heagerty, R.A. Malik, Diabetic cardiomyopathy, Clin. Sci. 116 (10) (2009) 741–760.

[11] T. van de Weijer, V.B. Schrauwen-Hinderling, P. Schrauwen, Lipotoxicity in type 2 diabetic cardiomyopathy, Cardiovasc Res. 92 (1) (2011) 10–18.

[12] F. Fiordaliso, R. Bianchi, L. Staszewsky, I. Cuccovillo, M. Doni, T. Laragione, M. Salio, C. Savino, S. Melucci, F. Santangelo, E. Scanziani, S. Masson, P. Ghezzi, R. Latini, Antioxidant treatment attenuates hyperglycemia-induced cardiomyocyte death in rats, J. Mol. Cell Cardiol. 37 (5) (2004) 959–968.

[13] Z.V. Wang, J.A. Hill, Diabetic cardiomyopathy: catabolism driving metabolism, Circulation 131 (9) (2015) 771–773.

[14] A. Planavila, J.C. Laguna, M. Vázquez-Carrera, Nuclear factor-kappaB activation leads to down-regulation of fatty acid oxidation during cardiac hypertrophy, J. Biol. Chem. 280 (17) (2005) 17464–17471.

[15] A. Planavila, R. Rodríguez-Calvo, M. Jove, L. Michalik, W. Wahli, J.C. Laguna, M. Vázquez-Carrera, Peroxisome proliferator-activated receptor beta/delta activation inhibits hypertrophy in neonatal rat cardiomyocytes, Cardiovasc Res. 65 (4) (2005) 832–841.

[16] J.N. Feige, L. Gelman, L. Michalik, B. Desvergne, W. Wahli, From molecular action to physiological outputs: peroxisome proliferator-activated receptors are nuclear receptors at the crossroads of key cellular functions, Prog. Lipid Res. 45 (2) (2006) 120–159.

[17] S.K. Verma, V. Deshmukh, P. Liu, C.A. Nutter, R. Espejo, M.L. Hung, G.S. Wang, G.W. Yeo, M.N. Kuyumcu-Martinez, Reactivation of fetal splicing programs in diabetic hearts is mediated by protein kinase C signaling, J. Biol. Chem. 288 (49) (2013) 35372–35386.

[18] S.B. Gurley, S.E. Clare, K.P. Snow, A. Hu, T.W. Meyer, T.M. Coffman, Impact of genetic background on nephropathy in diabetic mice, Am. J. Physiol. Ren. Physiol. 290 (1) (2006) F214–F222.

[19] E. Barroso, R. Rodriguez-Calvo, L. Serrano-Marco, A.M. Astudillo, J. Balsinde, X. Palomer, M. Vazquez-Carrera, The PPAR{beta}/{delta} activator GW501516 prevents the down-regulation of AMPK caused by a high-fat diet in liver and amplifies the PGC-1{alpha}-Lipin 1-PPAR{alpha} pathway leading to increased fatty acid oxidation, Endocrinology 152 (5) (2011) 1848–1859.

[20] J.C. McGrath, E. Lilley, Implementing guidelines on reporting research using animals (ARRIVE etc.): new requirements for publication in BJP, Br. J. Pharm. 172 (13) (2015) 3189–3193.

[21] X. Palomer, M.S. Roman-Azcona, J. Pizarro-Delgado, A. Planavila, F. Villarroya, B. Valenzuela-Alcaraz, F. Crispi, A. Sepulveda-Martinez, I. Miguel-Escalada, J. Ferrer, J.F. Nistal, R. Garcia, M.M. Davidson, E. Barroso, M. Vazquez-Carrera, SIRT3-mediated inhibition of FOS through histone H3 deacetylation prevents cardiac fibrosis and inflammation, Signal Transduct. Target Ther. 5 (2020) 14.

[22] X. Palomer, E. Capdevila-Busquets, D. Álvarez-Guardia, E. Barroso, M. Pallas, A. Camins, M.M. Davidson, A. Planavila, F. Villarroya, M. Vazquez-Carrera, Resveratrol induces nuclear factor-kappaB activity in human cardiac cells, Int J. Cardiol. 167 (6) (2013) 2507–2516.

[23] B.C. Yu, C.K. Chang, H.Y. Ou, K.C. Cheng, J.T. Cheng, Decrease of peroxisome proliferator-activated receptor delta expression in cardiomyopathy of streptozotocin-induced diabetic rats, Cardiovasc Res. 80 (1) (2008) 78–87.

[24] Y. Matsushita, D. Ogawa, J. Wada, N. Yamamoto, K. Shikata, C. Sato, H. Tachibana, N. Toyota, H. Makino, Activation of peroxisome proliferator-activated receptor delta inhibits streptozotocin-induced diabetic nephropathy through anti-inflammatory mechanisms in mice, Diabetes 60 (3) (2011) 960–968.

[25] C. Chandramouli, M.E. Reichelt, C.L. Curl, U. Varma, L.A. Bienvenu, P. Koutsifeli, A.J.A. Raaijmakers, M.J. De Blasio, C.X. Qin, A.J. Jenkins, R.H. Ritchie, K. M. Mellor, L.M.D. Delbridge, Diastolic dysfunction is more apparent in STZ-induced diabetic female mice, despite less pronounced hyperglycemia, Sci. Rep. 8 (1) (2018) 2346.

[26] R.H. Ritchie, E.D. Abel, Basic Mechanisms of Diabetic Heart Disease, Circ. Res 126 (11) (2020) 1501–1525.

[27] Q.A.J. Hagdorn, G.P.L. Bossers, A.C. Koop, A. Piek, T.R. Eijgenraam, D.E. van der Feen, H.H.W. Sillje, R.A. de Boer, R.M.F. Berger, A novel method optimizing the normalization of cardiac parameters in small animal models: the importance of dimensional indexing, Am. J. Physiol. Heart Circ. Physiol. 316 (6) (2019) H1552–H1557.

[28] R.B. Devereux, D.R. Alonso, E.M. Lutas, G.J. Gottlieb, E. Campo, I. Sachs, N. Reichek, Echocardiographic assessment of left ventricular hypertrophy: comparison to necropsy findings, Am. J. Cardiol. 57 (6) (1986) 450–458.

[29] C.M. Thomas, Q.C. Yong, R.M. Rosa, R. Seqqat, S. Gopal, D.E. Casarini, W. K. Jones, S. Gupta, K.M. Baker, R. Kumar, Cardiac-specific suppression of NF-kappaB signaling prevents diabetic cardiomyopathy via inhibition of the renin-angiotensin system, Am. J. Physiol. Heart Circ. Physiol. 307 (7) (2014) H1036–H1045.

[30] Y. Ti, G.L. Xie, Z.H. Wang, X.L. Bi, W.Y. Ding, J. Wang, G.H. Jiang, P.L. Bu, Y. Zhang, M. Zhong, W. Zhang, TRB3 gene silencing alleviates diabetic cardiomyopathy in a type 2 diabetic rat model, Diabetes 60 (11) (2011) 2963–2974.

[31] R. Guo, Z. Wu, J. Jiang, C. Liu, B. Wu, X. Li, T. Li, H. Mo, S. He, S. Li, H. Yan, R. Huang, Q. You, K. Wu, New mechanism of lipotoxicity in diabetic cardiomyopathy: deficiency of endogenous H2S production and ER stress, Mech. Ageing Dev. 162 (2017) 46–52.

[32] B. Wu, J. Lin, J. Luo, D. Han, M. Fan, T. Guo, L. Tao, M. Yuan, F. Yi, Dihydromyricetin protects against diabetic cardiomyopathy in streptozotocin-induced diabetic mice, Biomed. Res. Int. 2017 (2017) 3764370.

[33] L. Dai, Y. Xie, W. Zhang, X. Zhong, M. Wang, H. Jiang, Z. He, X. Liu, H. Zeng, H. Wang, Weighted gene Co-expression network analysis identifies ANGPTL4 as a key regulator in diabetic cardiomyopathy via FAK/SIRT3/ROS pathway in cardiomyocyte, Front Endocrinol. (Lausanne) 12 (2021) 705154.

[34] M. Long, M. Cheng, Small extracellular vesicles associated miRNA in myocardial fibrosis, Biochem Biophys. Res. Commun. 727 (2024) 150336.

[35] Y.L. Shevchenko, A.V. Plotnitsky, D.S. Ulbashev, Immobilizing interstitial cardiac fibrosis, Cardiol. Res. 14 (2) (2023) 123–132.

[36] I. Tuleta, N.G. Frangogiannis, Fibrosis of the diabetic heart: clinical significance, molecular mechanisms, and therapeutic opportunities, Adv. Drug Deliv. Rev. 176 (2021) 113904.

[37] N.E. Buroker, J. Barboza, J.Y. Huang, The IkappaBalpha gene is a peroxisome proliferator-activated receptor cardiac target gene, FEBS J. 276 (12) (2009) 3247–3255.

[38] X. Palomer, E. Barroso, M. Zarei, G. Botteri, M. Vazquez-Carrera, PPARbeta/delta and lipid metabolism in the heart, Biochim Biophys. Acta 1861 (10) (2016) 1569–1578.

[39] A. Planavila, R. Rodriguez-Calvo, M. Jove, L. Michalik, W. Wahli, J.C. Laguna, M. Vazquez-Carrera, Peroxisome proliferator-activated receptor beta/delta activation inhibits hypertrophy in neonatal rat cardiomyocytes, Cardiovasc Res. 65 (4) (2005) 832–841.

[40] A. Planavila, J.C. Laguna, M. Vazquez-Carrera, Nuclear factor-kappaB activation leads to down-regulation of fatty acid oxidation during cardiac hypertrophy, J. Biol. Chem. 280 (17) (2005) 17464–17471.

[41] D. Álvarez-Guardia, X. Palomer, T. Coll, L. Serrano, R. Rodriguez-Calvo, M. M. Davidson, M. Merlos, I. El Kochairi, L. Michalik, W. Wahli, M. Vazquez-Carrera, PPARbeta/delta activation blocks lipid-induced inflammatory pathways in mouse heart and human cardiac cells, Biochim Biophys. Acta 1811 (1) (2011) 59–67.

[42] H.L. Li, R. Yin, D. Chen, D. Liu, D. Wang, Q. Yang, Y.G. Dong, Long-term activation of adenosine monophosphate-activated protein kinase attenuates pressure-overload-induced cardiac hypertrophy, J. Cell Biochem. 100 (5) (2007) 1086–1099.

[43] L. Serrano-Marco, E. Barroso, K. El, I, X. Palomer, L. Michalik, W. Wahli, M. Vazquez-Carrera, The peroxisome proliferator-activated receptor (PPAR) beta/delta agonist GW501516 inhibits IL-6-induced signal transducer and activator of transcription 3 (STAT3) activation and insulin resistance in human liver cells, Diabetologia 55 (3) (2012) 743–751.

[44] J. Gu, S. Wang, H. Guo, Y. Tan, Y. Liang, A. Feng, Q. Liu, C. Damodaran, Z. Zhang, B.B. Keller, C. Zhang, L. Cai, Inhibition of p53 prevents diabetic cardiomyopathy by preventing early-stage apoptosis and cell senescence, reduced glycolysis, and impaired angiogenesis, Cell Death Dis. 9 (2) (2018) 82.

[45] X. Palomer, E. Capdevila-Busquets, G. Botteri, M.M. Davidson, C. Rodriguez, J. Martinez-Gonzalez, F. Vidal, E. Barroso, T.O. Chan, A.M. Feldman, M. Vazquez-

Carrera, miR-146a targets c-Fos expression in human cardiac cells, Dis. Model Mech. 8 (9) (2015) 1081–1091.
[46] N. Gurusamy, K. Watanabe, M. Ma, P. Prakash, K. Hirabayashi, S. Zhang, A. J. Muslin, M. Kodama, Y. Aizawa, Glycogen synthase kinase 3beta together with 14-3-3 protein regulates diabetic cardiomyopathy: effect of losartan and tempol, FEBS Lett. 580 (8) (2006) 1932–1940.
[47] R.A. Thandavarayan, V.V. Giridharan, F.R. Sari, S. Arumugam, P.T. Veeraveedu, G.N. Pandian, S.S. Palaniyandi, M. Ma, K. Suzuki, N. Gurusamy, K. Watanabe, Depletion of 14-3-3 protein exacerbates cardiac oxidative stress, inflammation and remodeling process via modulation of MAPK/NF-kB signaling pathways after streptozotocin-induced diabetes mellitus, Cell Physiol. Biochem. 28 (5) (2011) 911–922.
[48] F. Yang, Y. Qin, Y. Wang, A. Li, J. Lv, X. Sun, H. Che, T. Han, S. Meng, Y. Bai, L. Wang, LncRNA KCNQ1OT1 mediates pyroptosis in diabetic cardiomyopathy, Cell Physiol. Biochem 50 (4) (2018) 1230–1244.
[49] S. Kumar, S. Prasad, S.L. Sitasawad, Multiple antioxidants improve cardiac complications and inhibit cardiac cell death in streptozotocin-induced diabetic rats, PLoS One 8 (7) (2013) e67009.
[50] C. Besler, D. Lang, D. Urban, K.P. Rommel, M. von Roeder, K. Fengler, S. Blazek, R. Kandolf, K. Klingel, H. Thiele, A. Linke, G. Schuler, V. Adams, P. Lurz, Plasma and cardiac galectin-3 in patients with heart failure reflects both inflammation and fibrosis: implications for its use as a biomarker, Circ. Heart Fail 10 (3) (2017) e003804.
[51] G. Radosavljevic, V. Volarevic, I. Jovanovic, M. Milovanovic, N. Pejnovic, N. Arsenijevic, D.K. Hsu, M.L. Lukic, The roles of Galectin-3 in autoimmunity and tumor progression, Immunol. Res. 52 (1-2) (2012) 100–110.
[52] F. Liu, R. Song, Y. Feng, J. Guo, Y. Chen, Y. Zhang, T. Chen, Y. Wang, Y. Huang, C. Y. Li, C. Cao, Y. Zhang, X. Hu, R.P. Xiao, Upregulation of MG53 induces diabetic cardiomyopathy through transcriptional activation of peroxisome proliferation-activated receptor alpha, Circulation 131 (9) (2015) 795–804.
[53] J. Guo, F. Jia, Y. Jiang, Q. Li, Y. Yang, M. Xiao, H. Xiao, Potential role of MG53 in the regulation of transforming-growth-factor-beta1-induced atrial fibrosis and vulnerability to atrial fibrillation, Exp. Cell Res. 362 (2) (2018) 436–443.
[54] X. Chen, J. Su, J. Feng, L. Cheng, Q. Li, C. Qiu, Q. Zheng, TRIM72 contributes to cardiac fibrosis via regulating STAT3/Notch-1 signaling, J. Cell Physiol. 234 (10) (2019) 17749–17756.
[55] E.N. Stujanna, N. Murakoshi, K. Tajiri, D. Xu, T. Kimura, R. Qin, D. Feng, S. Yonebayashi, Y. Ogura, F. Yamagami, A. Sato, A. Nogami, K. Aonuma, Rev-erb agonist improves adverse cardiac remodeling and survival in myocardial infarction through an anti-inflammatory mechanism, PLoS One 12 (12) (2017) e0189330.
[56] L. Zhang, R. Zhang, C.L. Tien, R.E. Chan, K. Sugi, C. Fu, A.C. Griffin, Y. Shen, T. P. Burris, X. Liao, M.K. Jain, REV-ERBalpha ameliorates heart failure through transcription repression, JCI Insight 2 (17) (2017) e95177.
[57] B.E. Teunissen, P.J. Smeets, P.H. Willemsen, L.J. De Windt, G.J. Van der Vusse, M. Van Bilsen, Activation of PPARdelta inhibits cardiac fibroblast proliferation and the transdifferentiation into myofibroblasts, Cardiovasc Res. 75 (3) (2007) 519–529.
[58] C. Liu, S.T. Lim, M.H.Y. Teo, M.S.Y. Tan, M.D. Kulkarni, B. Qiu, A. Li, S. Lal, C. G. Dos Remedios, N.S. Tan, W. Wahli, M.A. Ferenczi, W. Song, W. Hong, X. Wang, Collaborative Regulation of LRG1 by TGF-beta1 and PPAR-beta/delta modulates chronic pressure overload-induced cardiac fibrosis, Circ. Heart Fail 12 (12) (2019) e005962.
[59] M. Ridwan, H. Dimiati, M. Syukri, R. Lesmana, Potential molecular mechanism underlying cardiac fibrosis in diabetes mellitus: a narrative review, Egypt Heart J. 75 (1) (2023) 46.
[60] P. Kong, P. Christia, N.G. Frangogiannis, The pathogenesis of cardiac fibrosis, Cell Mol. Life Sci. 71 (4) (2014) 549–574.
[61] A. Kashiwagi, S. Araki, H. Maegawa, Sodium-glucose cotransporter 2 inhibitors represent a paradigm shift in the prevention of heart failure in type 2 diabetes patients, J. Diabetes Invest. 12 (1) (2021) 6–20.
[62] W. Luo, L. Huang, J. Wang, F. Zhuang, Z. Xu, H. Yin, Y. Qian, G. Liang, C. Zheng, Y. Wang, Inhibition of EGFR-STAT3 attenuates cardiomyopathy in streptozotocin-induced type 1 diabetes, J. Endocrinol. 242 (3) (2019) 199–210.
[63] J. Wang, C. Qian, Y. Chen, T. Jin, Y. Jiang, L. Huang, X. Fu, D. Yang, L. Jin, B. Jin, Y. Wang, beta-elemene alleviates hyperglycemia-induced cardiac inflammation and remodeling by inhibiting the JAK/STAT3-NF-kappaB pathway, Phytomedicine 119 (2023) 154987.
[64] X. Sun, R.C. Chen, Z.H. Yang, G.B. Sun, M. Wang, X.J. Ma, L.J. Yang, X.B. Sun, Taxifolin prevents diabetic cardiomyopathy in vivo and in vitro by inhibition of oxidative stress and cell apoptosis, Food Chem. Toxicol. 63 (2014) 221–232.
[65] S.H. Lo, C.T. Hsu, H.S. Niu, C.S. Niu, J.T. Cheng, Z.C. Chen, Ginsenoside Rh2 Improves Cardiac Fibrosis via PPARdelta-STAT3 Signaling in Type 1-Like Diabetic Rats, Int J. Mol. Sci. 18 (7) (2017) 1364.
[66] B. Dai, M. Cui, M. Zhu, W.L. Su, M.C. Qiu, H. Zhang, STAT1/3 and ERK1/2 synergistically regulate cardiac fibrosis induced by high glucose, Cell Physiol. Biochem 32 (4) (2013) 960–971.
[67] N.H. Moritani, S. Kubota, T. Eguchi, T. Fukunaga, T. Yamashiro, T. Takano-Yamamoto, H. Tahara, K. Ohyama, T. Sugahara, M. Takigawa, Interaction of AP-1 and the ctgf gene: a possible driver of chondrocyte hypertrophy in growth cartilage, J. Bone Min. Metab. 21 (4) (2003) 205–210.
[68] K.C. Cheng, W.T. Chang, Y. Li, Y.Z. Cheng, J.T. Cheng, Z.C. Chen, GW0742 activates peroxisome proliferator-activated receptor delta to reduce free radicals and alleviate cardiac hypertrophy induced by hyperglycemia in cultured H9c2 cells, J. Cell Biochem 119 (11) (2018) 9532–9542.
[69] W.T. Chang, J.T. Cheng, Z.C. Chen, Telmisartan improves cardiac fibrosis in diabetes through peroxisome proliferator activated receptor delta (PPARdelta): from bedside to bench, Cardiovasc Diabetol. 15 (1) (2016) 113.
[70] Y.J. Liang, S.A. Chen, J.H. Jian, Peroxisome proliferator-activated receptor delta downregulates the expression of the receptor for advanced glycation end products and pro-inflammatory cytokines in the kidney of streptozotocin-induced diabetic mice, Eur. J. Pharm. Sci. 43 (1-2) (2011) 65–70.
[71] C.N. Palmer, M.H. Hsu, K.J. Griffin, J.L. Raucy, E.F. Johnson, Peroxisome proliferator activated receptor-alpha expression in human liver, Mol. Pharm. 53 (1) (1998) 14–22.
[72] J.W. Lawrence, Y. Li, S. Chen, J.G. DeLuca, J.P. Berger, D.R. Umbenhauer, D. E. Moller, G. Zhou, Differential gene regulation in human versus rodent hepatocytes by peroxisome proliferator-activated receptor (PPAR) alpha. PPAR alpha fails to induce peroxisome proliferation-associated genes in human cells independently of the level of receptor expresson, J. Biol. Chem. 276 (34) (2001) 31521–31527.
[73] T. Miki, S. Yuda, H. Kouzu, T. Miura, Diabetic cardiomyopathy: pathophysiology and clinical features, Heart Fail Rev. 18 (2) (2013) 149–166.
[74] W. Yu, B. Gao, N. Li, J. Wang, C. Qiu, G. Zhang, M. Liu, R. Zhang, C. Li, G. Ji, Y. Zhang, Sirt3 deficiency exacerbates diabetic cardiac dysfunction: role of Foxo3A-Parkin-mediated mitophagy, Biochim Biophys. Acta Mol. Basis Dis. 1863 (8) (2017) 1973–1983.
[75] H. Hu, M. Tian, C. Ding, S. Yu, The C/EBP homologous protein (CHOP) transcription factor functions in endoplasmic reticulum stress-induced apoptosis and microbial infection, Front Immunol. 9 (2018) 3083.
[76] G. Frati, L. Schirone, I. Chimenti, D. Yee, G. Biondi-Zoccai, M. Volpe, S. Sciarretta, An overview of the inflammatory signalling mechanisms in the myocardium underlying the development of diabetic cardiomyopathy, Cardiovasc Res. 113 (4) (2017) 378–388.
[77] K. Shimizu, S. Takahama, Y. Endo, T. Sawasaki, Stress-inducible caspase substrate TRB3 promotes nuclear translocation of procaspase-3, PLoS One 7 (8) (2012) e42721.
[78] Z. Li, T. Zhang, H. Dai, G. Liu, H. Wang, Y. Sun, Y. Zhang, Z. Ge, Involvement of endoplasmic reticulum stress in myocardial apoptosis of streptozocin-induced diabetic rats, J. Clin. Biochem Nutr. 41 (1) (2007) 58–67.
[79] T. Hamid, S.Z. Guo, J.R. Kingery, X. Xiang, B. Dawn, S.D. Prabhu, Cardiomyocyte NF-kappaB p65 promotes adverse remodelling, apoptosis, and endoplasmic reticulum stress in heart failure, Cardiovasc Res. 89 (1) (2011) 129–138.
[80] P. Puthanveetil, D. Zhang, Y. Wang, F. Wang, A. Wan, A. Abrahani, B. Rodrigues, Diabetes triggers a PARP1 mediated death pathway in the heart through participation of FoxO1, J. Mol. Cell Cardiol. 53 (5) (2012) 677–686.
[81] H. Sakuma, M. Yamamoto, M. Okumura, T. Kojima, T. Maruyama, K. Yasuda, High glucose inhibits apoptosis in human coronary artery smooth muscle cells by increasing bcl-xL and bfl-1/A1, Am. J. Physiol. Cell Physiol. 283 (2) (2002) C422–C428.
[82] S.G. Tang, X.Y. Liu, J.M. Ye, T.T. Hu, Y.Y. Yang, T. Han, W. Tan, Isosteviol ameliorates diabetic cardiomyopathy in rats by inhibiting ERK and NF-kappaB signaling pathways, J. Endocrinol. 238 (1) (2018) 47–60.
[83] G. Zuo, X. Ren, X. Qian, P. Ye, J. Luo, X. Gao, J. Zhang, S. Chen, Inhibition of JNK and p38 MAPK-mediated inflammation and apoptosis by ivabradine improves cardiac function in streptozotocin-induced diabetic cardiomyopathy, J. Cell Physiol. 234 (2) (2019) 1925–1936.
[84] L. Wang, H. Wu, Y. Deng, S. Zhang, Q. Wei, Q. Yang, S. Piao, W. Bei, X. Rong, J. Guo, FTZ Ameliorates Diabetic Cardiomyopathy by Inhibiting Inflammation and Cardiac Fibrosis in the Streptozotocin-Induced Model, Evid. Based Complement Altern. Med. 2021 (2021) 5582567.
[85] Z. Zhang, Z. Yang, S. Wang, X. Wang, J. Mao, Targeting MAPK-ERK/JNK pathway: a potential intervention mechanism of myocardial fibrosis in heart failure, Biomed. Pharm. 173 (2024) 116413.
[86] Q. Zhang, L. Wang, S. Wang, H. Cheng, L. Xu, G. Pei, Y. Wang, C. Fu, Y. Jiang, C. He, Q. Wei, Signaling pathways and targeted therapy for myocardial infarction, Signal Transduct. Target Ther. 7 (1) (2022) 78.
[87] Y.G. Lu, H. Tan, Q. Ma, X.X. Li, J. Cui, X. Zhang, X.L. Liang, Y.Q. Tie, SH2 domain-containing protein tyrosine phosphatase-2 (SHP-2) prevents cardiac remodeling after myocardial infarction through ERK/SMAD signaling pathway, Hum. Cell 34 (2) (2021) 325–334.
[88] C.H. Lo, L.C. Li, S.F. Yang, C.F. Tsai, Y.T. Chuang, H.J. Chu, K.C. Ueng, MicroRNA Let-7a, -7e and -133a attenuate hypoxia-induced atrial fibrosis via targeting collagen expression and the JNK pathway in HL1 cardiomyocytes, Int. J. Mol. Sci. 23 (17) (2022).
[89] S. Huo, B. Li, J. Du, X. Zhang, J. Zhang, Q. Wang, M. Song, Y. Li, Dibutyl phthalate induces liver fibrosis via p38MAPK/NF-kappaB/NLRP3-mediated pyroptosis, Sci. Total Environ. 897 (2023) 165500.
[90] N. Moran, p38 kinase inhibitor approved for idiopathic pulmonary fibrosis, Nat. Biotechnol. 29 (4) (2011) 301.
[91] W. Zou, S. Liu, D. Ye, G. Bai, M. Guo, R. Sun, P. Ran, PM2.5 induces lung inflammation and fibrosis via airway smooth muscle cell expression of the Wnt5a/JNK pathway, J. Thorac. Dis. 15 (11) (2023) 6094–6105.
[92] S.C. Ou, K.J. Bai, W.H. Cheng, J.Y. Chen, C.H. Lin, H.C. Wen, B.C. Chen, TGF-beta Induced CTGF expression in human lung epithelial cells through ERK, ADAM17, RSK1, and C/EBPbeta pathways, Int J. Mol. Sci. 21 (23) (2020).
[93] Y.H. Juan, Y.L. Yu, Y.P. Tsai, C.C. Lee, Y.S. Chen, Y.H. Ting, J.P. Tsai, Y.H. Hsieh, Alpha-mangostin alleviate renal interstitial fibrosis via suppression of TGF-beta1/Smad/ERK signaling axis in vitro and in vivo, Biochem Pharm. 218 (2023) 115935.

[94] J. Li, S. Jin, M.T. Barati, S. Rane, Q. Lin, Y. Tan, L. Cai, M.J. Rane, ERK and p38 MAPK inhibition controls NF-E2 degradation and profibrotic signaling in renal proximal tubule cells, Life Sci. 287 (2021) 120092.
[95] A. Cordova-Casanova, M. Cruz-Soca, J. Chun, J.C. Casar, E. Brandan, Activation of the ATX/LPA/LPARs axis induces a fibrotic response in skeletal muscle, Matrix Biol. 109 (2022) 121–139.
[96] E. Mills, L.A. O'Neill, Succinate: a metabolic signal in inflammation, Trends Cell Biol. 24 (5) (2014) 313–320.
[97] N. Lin, H. Lin, Q. Yang, W. Lu, Z. Sun, S. Sun, L. Meng, J. Chi, H. Guo, SGLT1 Inhibition attenuates apoptosis in diabetic cardiomyopathy via the JNK and p38 pathway, Front Pharm. 11 (2020) 598353.
[98] Z. Xu, J. Sun, Q. Tong, Q. Lin, L. Qian, Y. Park, Y. Zheng, The Role of ERK1/2 in the development of diabetic cardiomyopathy, Int. J. Mol. Sci. 17 (12) (2016).
[99] G.S.D. Purvis, F. Chiazza, J. Chen, R. Azevedo-Loiola, L. Martin, D.H.M. Kusters, C. Reutelingsperger, N. Fountoulakis, L. Gnudi, M.M. Yaqoob, M. Collino, C. Thiemermann, E. Solito, Annexin A1 attenuates microvascular complications through restoration of Akt signalling in a murine model of type 1 diabetes, Diabetologia 61 (2) (2018) 482–495.
[100] G.B. Singh, S.K. Raut, S. Khanna, A. Kumar, S. Sharma, R. Prasad, M. Khullar, MicroRNA-200c modulates DUSP-1 expression in diabetes-induced cardiac hypertrophy, Mol. Cell Biochem. 424 (1-2) (2017) 1–11.
[101] Q.G. Karwi, K.L. Ho, S. Pherwani, E.B. Ketema, Q. Sun, G.D. Lopaschuk, Concurrent diabetes and heart failure: interplay and novel therapeutic approaches, Cardiovasc Res. 118 (3) (2022) 686–715.
[102] D.V. Chistyakov, A.A. Astakhova, S.V. Goriainov, M.G. Sergeeva, Comparison of PPAR ligands as modulators of resolution of inflammation, via their influence on cytokines and oxylipins release in astrocytes, Int. J. Mol. Sci. 21 (24) (2020) 9577.